Article

Neuron

Multimodal and Site-Specific Plasticity of Amygdala Parvalbumin Interneurons after Fear Learning

Highlights

- Lateral (LA) but not basal amygdala (BA) PV-INs receive potent afferent excitation
- PV-INs in LA but not BA mediate feedforward inhibition onto principal neurons
- Fear conditioning modulates synaptic input to PV-INs in a nucleus-specific manner
- PV-INs reduce GABA release onto LA principal neurons after fear conditioning

Authors

Elizabeth K. Lucas, Anita M. Jegarl, Hirofumi Morishita, Roger L. Clem

Correspondence

roger.clem@mssm.edu

In Brief

Lucas et al. describe persistent downregulation of neurotransmission in parvalbumin interneurons in the basolateral amygdala after fear memory encoding. This inhibitory plasticity may facilitate subsequent amygdala recruitment by sensory stimuli.

Lucas et al., 2016, Neuron *91*, 629–643
August 3, 2016
http://dx.doi.org/10.1016/j.neuron.2016.06.032

CellPress

Neuron
Article

Multimodal and Site-Specific Plasticity of Amygdala Parvalbumin Interneurons after Fear Learning

Elizabeth K. Lucas,[1] Anita M. Jegarl,[1] Hirofumi Morishita,[1,2] and Roger L. Clem[1,2,*]
[1]Fishberg Department of Neuroscience and the Friedman Brain Institute, Icahn School of Medicine at Mount Sinai, New York, NY 10029, USA
[2]Department of Psychiatry and the Friedman Brain Institute, Icahn School of Medicine at Mount Sinai, New York, NY 10029, USA
*Correspondence: roger.clem@mssm.edu
http://dx.doi.org/10.1016/j.neuron.2016.06.032

SUMMARY

Stimulus processing in fear conditioning is constrained by parvalbumin interneurons (PV-INs) through inhibition of principal excitatory neurons. However, the contributions of PV-IN microcircuits to input gating and long-term plasticity in the fear system remain unknown. Here we interrogate synaptic connections between afferent pathways, PV-INs, and principal excitatory neurons in the basolateral amygdala. We find that subnuclei of this region are populated two functionally distinct PV-IN networks. PV-INs in the lateral (LA), but not the basal (BA), amygdala possess complex dendritic arborizations, receive potent excitatory drive, and mediate feedforward inhibition onto principal neurons. After fear conditioning, PV-INs exhibit nucleus- and target-selective plasticity, resulting in persistent reduction of their excitatory input and inhibitory output in LA but not BA. These data reveal previously overlooked specializations of amygdala PV-INs and indicate specific circuit mechanisms for inhibitory plasticity during the encoding of associative fear memories.

INTRODUCTION

Aversive memories acquired by classical conditioning provide insight into emotional learning under normal conditions as well as pathological states, such as posttraumatic stress disorder (PTSD) (Mahan and Ressler, 2012). Cellular models of fear learning place a great deal of emphasis on amygdala excitatory neuronal plasticity (Janak and Tye, 2015; Johansen et al., 2011). However, many studies posit that co-regulation of excitation and inhibition may be important for network stability and that excitation:inhibition (E:I) imbalance may be a factor in some psychiatric conditions (Dorrn et al., 2010; House et al., 2011; Katagiri et al., 2007; Vogels et al., 2011). Notably, decreased GABA levels as well as GABA receptor binding and polymorphisms have been associated with PTSD (Bremner et al., 2000; Feusner et al., 2001; Geuze et al., 2008; Meyerhoff et al., 2014; Pennington et al., 2014; Rossi et al., 2009; Rosso et al., 2014), and reduced GABA levels are predictive of disease progression (Vaiva et al., 2006; Vaiva et al., 2004). Changes in inhibitory synaptic markers suggest that plasticity of GABAergic transmission in the basolateral amygdala may also be a feature of aversive memory formation under normal conditions (Chhatwal et al., 2005; Heldt and Ressler, 2007; Lin et al., 2011). Although ex vivo stimulation of amygdala brain slices has been shown to induce long-term plasticity in undefined GABAergic populations (Bauer and LeDoux, 2004; Mahanty and Sah, 1998; Polepalli et al., 2010; Shin et al., 2006; Szinyei et al., 2000), it remains unknown whether specific GABAergic cell types exhibit plasticity associated with emotional learning.

The majority of GABAergic synaptic inhibition throughout the forebrain is thought to originate from a heterogeneous population of locally projecting interneurons. Within the basolateral amygdala, more than half of inhibitory synapses formed onto principal excitatory neurons are associated with PV-INs (Muller et al., 2006), which are considered to exert powerful control over the firing of these cells through dense somatic and axo-axonic synaptic terminals (Hu et al., 2014). Recently, in vivo manipulations within the basolateral amygdala (Wolff et al., 2014) as well as neocortical regions (Courtin et al., 2014; Letzkus et al., 2011) have implicated PV-INs in fear acquisition and expression through cue-related inhibition and disinhibition of principal excitatory neurons. Therefore, it is important to understand the circuit mechanisms underlying PV-IN recruitment and resulting excitatory neuronal inhibition as well as to determine whether fear conditioning generates persistent alterations in PV-IN function.

We utilized parvalbumin-specific Cre driver mice as well as optogenetic-assisted electrophysiology to investigate the properties and experience-dependent plasticity of PV-IN microcircuits. We report that function and plasticity of PV-INs varies by nucleus location within basolateral amygdala and that fear conditioning leads to downregulation of PV-IN transmission predominantly within microcircuits that mediate feedforward inhibition from sensory afferent pathways.

RESULTS

Uniquely Robust Afferent Excitation of Lateral Amygdala PV-INs

To selectively target PV-INs for in vitro electrophysiology, we crossed R26-STOP-eYFP reporter mice to the PV-IRES-Cre driver line to selectively express enhanced yellow fluorescent

protein (eYFP) in PV-INs. Given a previous report that only ~60% of PV-positive cells in the basolateral amygdala co-express GABA (McDonald and Mascagni, 2001), we sought to determine the specificity of Cre-mediated recombination by quantifying double immunofluorescence staining with antibodies against parvalbumin and GABA (Figures 1A and S1). More than 90% of eYFP-positive cells in the basolateral amygdala co-expressed both PV and GABA (Figure S1), demonstrating that this Cre line is highly selective for GABAergic PV-INs in this brain region.

During classical conditioning, a benign auditory conditioned stimulus (CS) is paired with a naturally aversive unconditioned stimulus (US), forming an associative memory that links the CS and US. In vivo studies have found that amygdala PV-INs respond differentially to sensory stimulation with increased firing to auditory stimuli (Wolff et al., 2014) and decreased firing to footshock (Wolff et al., 2014) and other noxious stimuli (Bienvenu et al., 2012). However, it is unknown whether PV-INs are directly modulated by afferent pathways conveying CS activity. To address this question, we performed whole-cell recordings from PV-INs and neighboring principal neurons during stimulation of subcortical and cortical sensory afferent pathways, which traverse the internal and external capsules, respectively. We first investigated the input/output (I/O) relationship of compound postsynaptic currents consisting of monosynaptic excitatory postsynaptic currents (EPSCs) and disynaptic feedforward inhibitory postsynaptic currents (IPSCs) at increasing stimulus intensities (Figures 1B–1K). While there was no difference in the I/O slope of IPSCs between populations, the I/O relation of monosynaptic EPSCs from both subcortical and cortical afferents was far steeper in LA PV-INs compared to their glutamatergic neighbors (Figure 1G; two-way ANOVA, main effect of neuron type, $F_{(1,22)} = 30.89$, $p < 0.0001$), indicating far greater excitatory drive from these pathways in PV-INs. While converging excitation from the subcortical and cortical pathways to the LA is hypothesized to be a key mediator of learning-induced synaptic plasticity (Sigurdsson et al., 2007), cortical neurons also send axon collaterals to BA (Sah et al., 2003; Turner and Herkenham, 1991). To determine whether these inputs exhibit similar potency, we investigated the I/O relationship of BA cortical synaptic currents (Figures 1H–1K). Unlike in LA, PV-INs and principal neurons in BA exhibited similar I/O slope of both monosynaptic EPSCs and feedforward IPSCs (Figure 1K). We then calculated an index of I/O slopes (calculated as I/O slope $_{EPSC}$/ I/O slope $_{IPSC}$) as a measure of E:I balance for LA and BA neurons. PV-INs in LA exhibited greater E:I index compared to PV-INs in BA as well as to principal neurons in both nuclei (Figure 1L; two-way ANOVA, main effect of neuron type, $F_{(1,33)} = 27.13$, $p < 0.0001$; main effect of nucleus, $F_{(2,33)} = 3.76$, $p = 0.03$; interaction, $F_{(2,33)} = 6.47$, $p = 0.004$). Importantly, EPSC onset latency was similar across cells and nuclei (Figure 1M), indicating that these responses shared a monosynaptic mechanism.

To determine whether differences in PV-IN anatomy could account for nucleus-specific excitatory drive, we performed morphological reconstructions of biocytin-filled PV-INs (Figure 1N). While soma and primary dendrite characteristics were comparable between nuclei, PV-INs in LA possessed twice as many dendritic branches ($t_{(18)} = 3.09$, $p = 0.006$) as those in BA, resulting in increased dendritic length ($t_{(18)} = 2.27$, $p = 0.04$; Figure 1O). Furthermore, truncated dendrites were very infrequent and the total number of such artifacts was similar between nuclei (LA = 4; BA = 3), indicating that the observed differences in physiology and morphology were not attributable to slice preparation.

PV-INs Meditate Feedforward Inhibition in Lateral but Not Basal Amygdala

Given the potent excitatory drive onto LA PV-INs, we hypothesized that PV-INs may generate greater feedforward inhibition onto principal neurons in LA compared to BA. To test this hypothesis, we harnessed the power of optogenetics to silence PV-INs during afferent stimulation while recording feedforward IPSCs. Conditional expression of the GFP-tagged enhanced light-driven inhibitory proton pump Archaerhodopsin-3.0 (eArch3.0; Chow et al., 2010) in PV-IRES-Cre mice resulted in GFP expression in both the soma and axonal arbors of PV-INs (Figures S2A and S2B). Whole-cell recordings in eArch3.0-expressing cells confirmed yellow light-induced (λ = 590 nm) neuronal silencing (Figures S2C–S2E). Notably, PV-INs escaped voltage clamp and generated rebound action currents following light offset at every stimulus intensity (Figure S2C).

To evoke monosynaptic EPSCs and feedforward IPSCs, principal neurons were clamped at membrane potentials of −70 mV and 0 mV, respectively, during stimulation of subcortical and cortical afferents. Feedforward IPSCs were abolished by the $GABA_A$ receptor antagonist picrotoxin as well as the AMPA/kainate receptor antagonist CNQX (Figure 2B). In addition, the onset latency of feedforward IPSCs was delayed relative to EPSCs (independent samples t test, $t_{(36)} = 11.01$, $p < 0.0001$), consistent with a disynaptic circuit mechanism (Figure 2C).

Having validated our approach, we patched onto principal neurons in mice with conditional eArch3.0 expression in PV-INs and recorded feedforward IPSCs evoked by subcortical or cortical afferent stimulation in the presence or absence of yellow light (Figure 2A). Feedforward IPSCs from both pathways were attenuated by silencing PV-INs in LA (Figures 2D–2G; paired samples t test, subcortical: $t_{(13)} = 3.59$, $p = 0.003$; cortical: $t_{(7)} = 2.57$, $p = 0.03$). Consistent with low cortical excitatory drive onto BA PV-INs (Figure 1L), PV-IN silencing did not affect the amplitude of feedforward IPSCs in this nucleus (Figures 2I and 2J; paired samples t test, $t_{(11)} = 0.05$, $p = 0.96$).

Consistent with our observation of rebound action currents in eArch3.0-expressing cells (Figure S2C), we also observed corresponding rebound IPSCs in principal neurons at LED offset (Figures 2E, 2G, and 2J). Interestingly, we found that peak rebound amplitude positively correlated with reduction of feedforward IPSC amplitude by LED illumination (Figure 2H; linear regression, $F_{(1,20)} = 29.09$, $p < 0.0001$). Since rebound amplitude partly reflects the number of viable eArch3.0-infected PV-INs in our recording field, this further indicates that PV-INs are readily engaged in feedforward inhibition in the LA.

Fear Conditioning Induces Nucleus-Specific Alterations in PV-IN Synaptic Input

To determine whether fear learning alters PV-IN properties, we conducted whole-cell recordings in PV-INs after auditory fear conditioning, which entailed paired or unpaired presentations

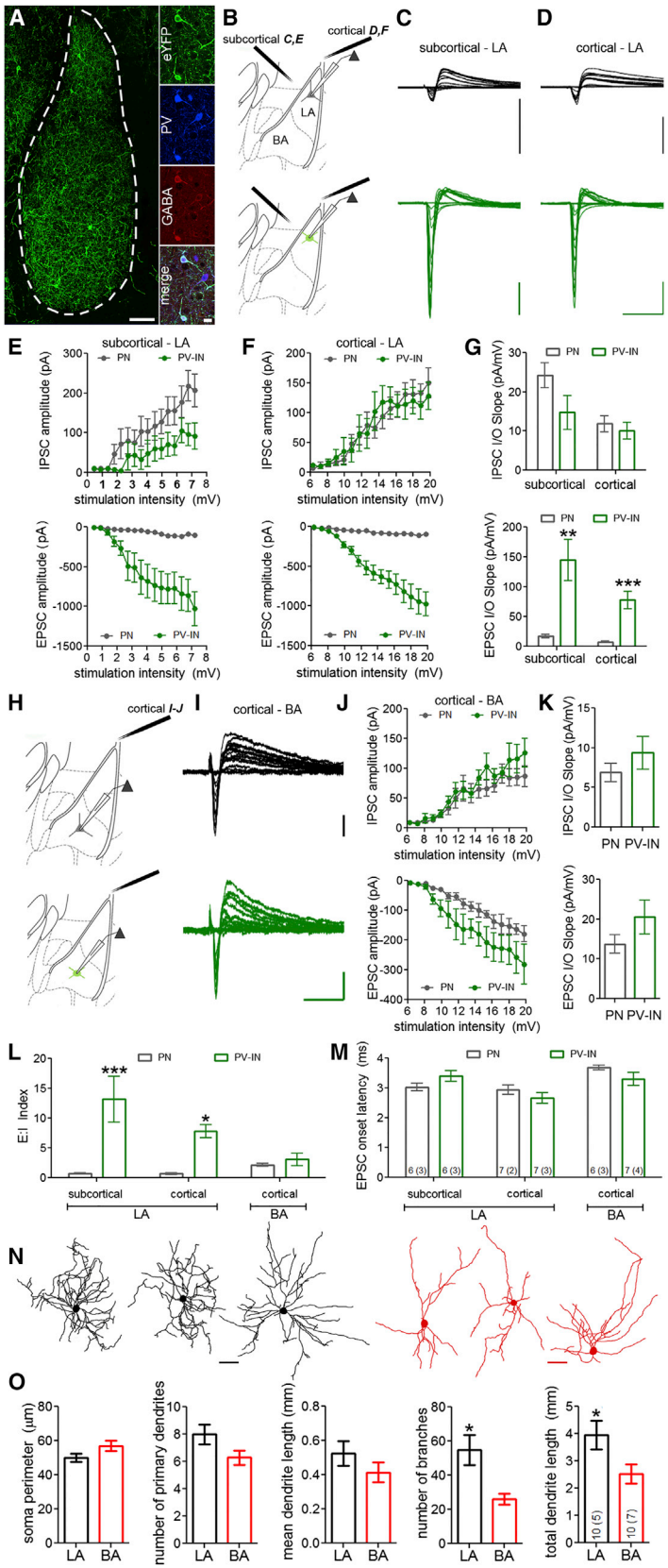

Figure 1. Lateral Amygdala Parvalbumin-Interneurons Receive Uniquely Potent Excitatory Drive

(A) To identify PV-INs for electrophysiological targeting, we crossed PV-IRES-Cre mice to R26-stop-eYFP reporter mice to express eYFP specifically in PV-INs. Double immunofluorescence staining with antibodies against PV (blue) and GABA (red) revealed that Cre-dependent eYFP (green) expression selectively labels PV-positive GABAergic neurons in the basolateral complex. Scales: left, 100 μm; right, 20 μm.

(B–D) Lateral amygdala PV-INs and neighboring principal neurons (PNs) respond to subcortical (C) and cortical (D) afferent stimulation with distinct biphasic synaptic responses, corresponding to monosynaptic EPSCs followed by disynaptic IPSCs. Scales: 500 pA × 40 ms.

(E and F) Input/output (I/O) relation of lateral amygdala EPSCs and IPSCs during increasing stimulus intensity.

(G) Slope of I/O relation for IPSC (top) and EPSC (bottom) components represented in (E) and (F).

(H and I) Basal amygdala PV-INs and neighboring PNs exhibit similar biphasic EPSC-IPSC responses during cortical afferent stimulation. Scales: 50 pA × 40 ms.

(J) I/O relation of basal amygdala EPSCs and IPSCs.

(K) Slope of I/O relation for IPSC (top) and EPSC (bottom) components represented in J.

(L) Excitatory:inhibitory (E:I) balance of biphasic responses for lateral and basal amygdala recordings. E:I index = I/O slope $_{EPSC}$/ I/O slope $_{IPSC}$.

(M) Similar onset latency for monosynaptic EPSC components across cells and nuclei.

(N) Representative reconstructions of biocytin-filled PV-INs from lateral (black) and basal (red) amygdala. Scales: 50 μm.

(O) Quantification of morphological reconstructions.

(B–M) Membrane potential was clamped at −50 mV for all recordings. n/group indicated on bar histogram in (M) ([C]–[M]) and (O).

(G, L, and M) Two-way ANOVA followed by Holm-Bonferroni.

(K and O) Independent samples t tests. *p < 0.05, **p < 0.005, and ***p < 0.0005. Data presented as mean ± SEM.

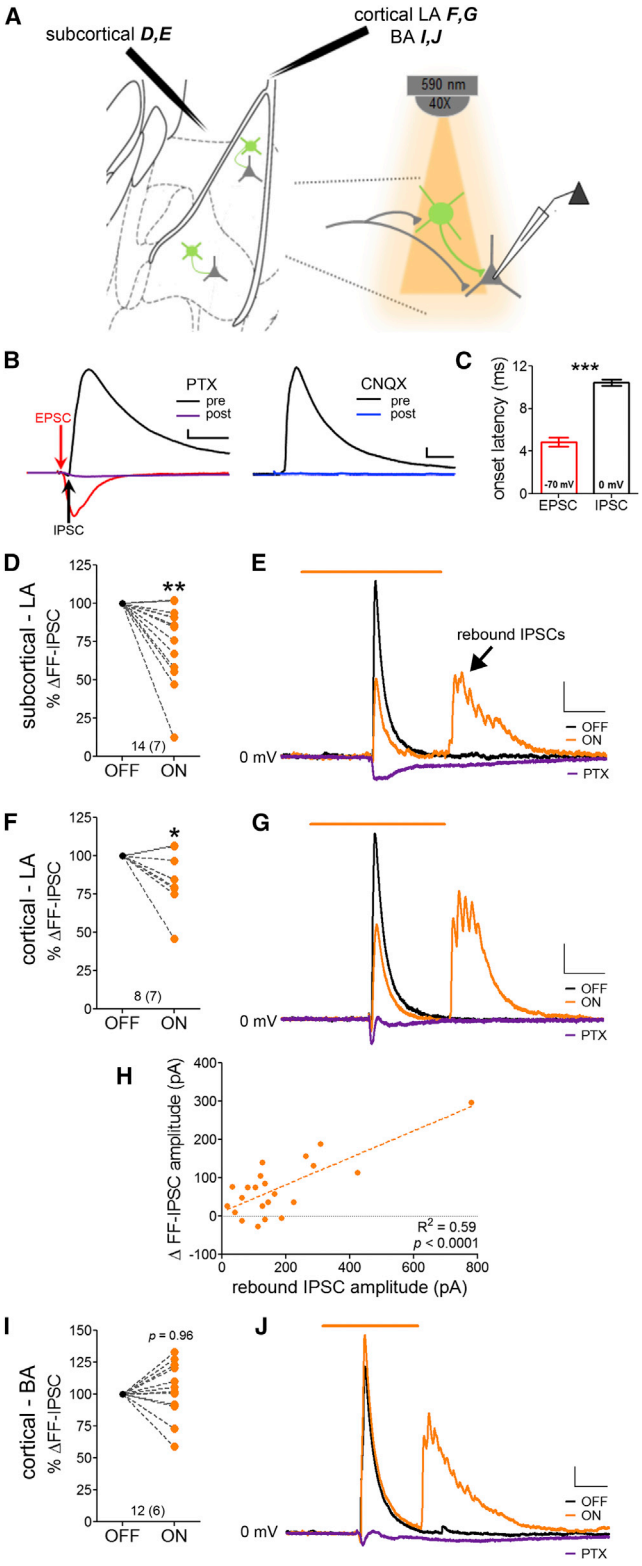

Figure 2. PV-INs Mediate Feedforward Inhibition in the Lateral but Not the Basal Amygdala

(A) Experimental design in (D)–(J). Subcortical ([D], [E]) and cortical (LA: [F], [G]; BA: [I], [J]) afferents were electrically stimulated to obtain monosynaptic EPSCs and disynaptic IPSCs in LA PNs during voltage clamp at −70 mV and 0 mV, respectively. Electrical stimulation alternated between light-off (n = 3) and light-on (n = 2) epochs (n = 10 sweeps per epoch).

(B) Example traces of monosynaptic excitatory (red trace; −70 mV) and disynaptic inhibitory (black trace; 0 mV) postsynaptic currents evoked from cortical afferents. Disynaptic IPSCs are blocked by the $GABA_A$ receptor antagonist picrotoxin (PTX; purple trace, left) and the AMPA/kainate receptor antagonist CNQX (blue trace, right). Scales: 70 pA × 20 ms.

(C) Onset latencies of monosynaptic EPSCs and disynaptic IPSCs, shown by arrows in (B).

(D–G) Silencing PV-INs attenuated the amplitude of disynaptic IPSCs evoked from subcortical ([D], representative traces in [E]) and cortical ([F], representative traces in [G]) afferent stimulation. Evoked IPSCs were blocked by PTX.

(H) Reduction of disynaptic IPSC peak amplitude is correlated with the rebound IPSC amplitude generated at LED offset in LA.

(I) PV-IN silencing did not affect the amplitude of disynaptic IPSCs evoked from cortical afferent stimulation in BA, representative traces in (J). Scales in (E), (G), and (J): 50 pA × 100 ms. n/group indicated on graphs.

(C) Independent samples t test.

(D, F, and I) Paired samples t test.

(H) Linear regression. *p < 0.05, **p < 0.005, and ***p < 0.0005. Data in (D), (F), and (I) are normalized to IPSC amplitude in the absence of LED stimulation. Data presented as mean ± SEM.

of an auditory tone (CS) and footshock (US). We confirmed that auditory fear was specific to the paired condition, since CS-evoked freezing was observed 24 hr later in mice that received paired but not unpaired training (Figure S3). All electrophysiological recordings were obtained 24 hr after training from a different set of animals in which retrieval was omitted in order to exclude the possibility of memory extinction or reconsolidation. An analysis of miniature (m) EPSCs and mIPSCs from paired, unpaired, and naive mice at this time point revealed nucleus-specific alterations in PV-INs that were correlated with auditory fear encoding (Figure 3). The frequency of mEPSCs differed between conditions in LA (one-way ANOVA, $F_{(2,22)} = 3.78$, $p = 0.04$) but not in BA (one-way ANOVA, $F_{(2,33)} = 2.34$, $p = 0.11$; Figures 3B–3D and 3I–3K). In LA PV-INs, mEPSC frequency was reduced in paired ($p = 0.008$), but not in unpaired ($p = 0.74$), mice compared to naive controls. In contrast, the frequency of mIPSCs differed between conditions in BA (one-way ANOVA, $F_{(2,32)} = 4.42$, $p = 0.02$) but not in LA (one-way ANOVA, $F_{(2,22)} = 0.31$, $p = 0.74$;Figures 3E–3G and 3L–3N). In BA PV-INs, mIPSC frequency was increased in paired ($p = 0.03$), but not unpaired ($p = 0.48$), mice relative to naive controls. Fear conditioning did not affect the amplitude or kinetics of mEPSCs or mIPSCs. However, independent of fear conditioning, these properties were strongly affected by nucleus location of PV-INs (Figure S4).

The above changes suggest that PV-INs are modulated by a nucleus-specific adjustment of their presynaptic input. Given robust excitation of PV-INs by amygdala afferents (Figure 1), we questioned whether excitatory presynaptic plasticity could be attributed to these pathways. As an assay of glutamate release probability, we measured the paired pulse ratio (PPR) of EPSCs evoked by subcortical and cortical stimulation. Consistent with decreased release probability, PPR was increased at both subcortical (repeated-measures ANOVA, main effect of group, $F_{(2,72)} = 26.23$, $p < 0.001$) and cortical (repeated-measures ANOVA, main effect of group, $F_{(2,104)} = 41.73$, $p < 0.001$) synapses in LA of mice that received paired

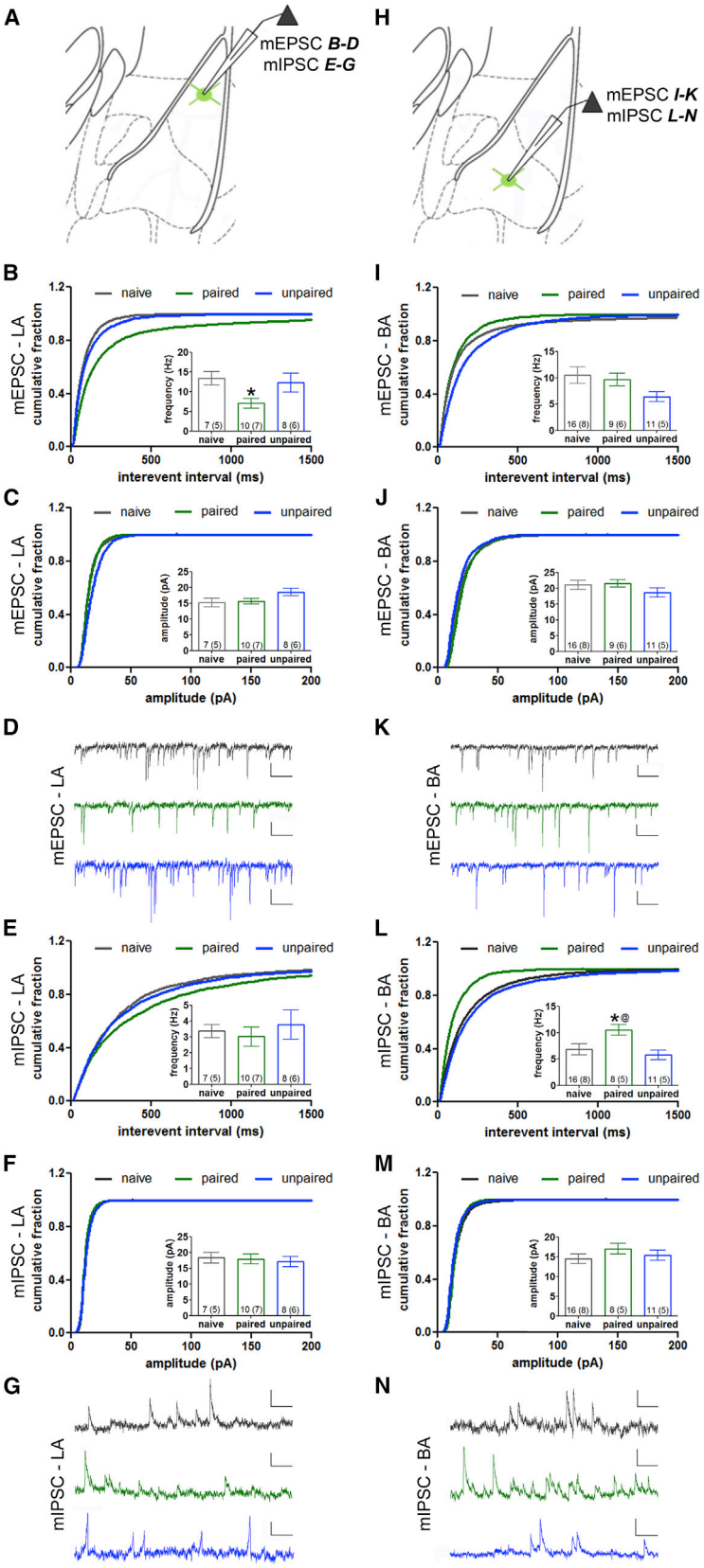

Figure 3. Auditory Fear Conditioning Induces Nucleus-Specific Remodeling of Synaptic Input onto PV-INs

Miniature postsynaptic currents were recorded in PV-INs with a low chloride internal solution, allowing for isolation of EPSCs and IPSCs at −60 mV and 0 mV, respectively.

(A) Schematic of LA miniature postsynaptic recordings in (B)–(G).

(B–D) Frequency (B) but not amplitude (C) of mEPSCs (representative traces in [D]) was reduced in LA PV-INs of mice that received paired, but not unpaired, training as compared to naive mice.

(E–G) The frequency (E) and amplitude (F) of mIPSCs was unaffected (representative traces in [G]).

(H) Schematic of BA miniature postsynaptic recordings in (I)–(N).

(I–K) The frequency (I) and amplitude (J) of mEPSCs (representative traces in K) in BA PV-INs were unaffected by training.

(L–N) The frequency (L) but not amplitude (M) of mIPSCs (representative traces in [N]) was increased after paired, but not unpaired, training compared to the naive condition. Scales: ([D], [G], [K]) 10 pA × 100 ms; [N] 20 pA × 100 ms. n/group indicated on bar histograms. One-way ANOVA followed by Fisher's LSD, *$p < 0.05$ naive versus paired, @ $p < 0.05$ paired versus unpaired. Data presented as mean ± SEM.

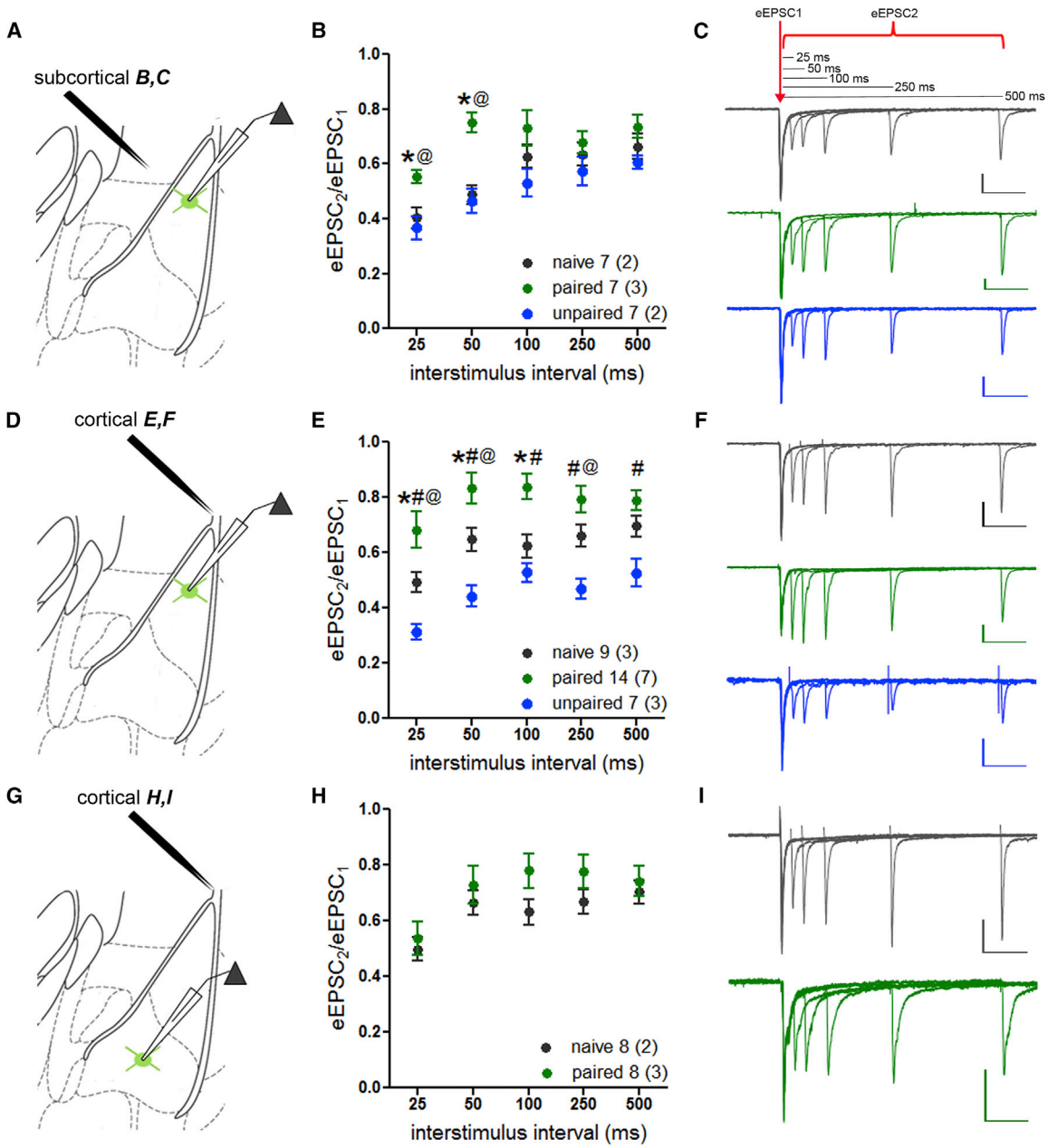

Figure 4. Reduced Afferent Input onto Lateral, but Not Basal, Amygdala PV-INs after Fear Memory Encoding

Release probability of excitatory subcortical and cortical inputs to PV-INs was assayed by paired-pulse stimulation of the internal (A) and external ([D], [G]) capsules, respectively.

(A–C) Paired-pulse ratio (PPR; $EPSC_2/EPSC_1$) of subcortical EPSCs was increased in LA PV-INs from mice that received paired training compared to both unpaired and naive conditions. Representative traces in (C).

(D–F) PPR of cortical EPSCs was increased in LA PV-INs in mice that received paired training compared to both naive and unpaired conditions. Representative traces in (F).

(G–I) PPR of cortical EPSCs was not altered by fear conditioning in BA PV-INs. Representative traces in (I). Scales: 80 pA × 100 ms. n/group indicated on graphs. Repeated-measures ANOVA followed by Holm-Bonferroni, *$p < 0.05$ naive versus paired, @ $p < 0.05$ paired versus unpaired, and # $p < 0.05$ naive versus unpaired. Data presented as mean ± SEM.

training compared to unpaired and naive controls (Figures 4A–4F). Interestingly, PPR was also decreased at cortical synapses after unpaired training (Figure 4E), but evidently this was not sufficient to enhance overall excitation onto LA PV-INs (Figure 3B). To determine whether presynaptic plasticity was nucleus specific, we measured PPR of cortical EPSCs in BA PV-INs. This

revealed no change in glutamate release in trained animals (Figures 4G–4I), consistent with a lack of modulation of mEPSC frequency by learning in BA PV-INs (Figure 3I).

Presynaptic Origins of Subcortical and Cortical Afferent Plasticity

Although electrical stimulation of the internal and external capsules is presumed to recruit glutamatergic axons from sensory thalamus and cortex, respectively, we sought to characterize this circuitry using region- and cell-selective tools. To determine the presynaptic origins of PV-IN innervation, we conducted unbiased Cre-dependent monosynaptic circuit tracing (Watabe-Uchida et al., 2012; Wickersham et al., 2007). AAVs encoding conditional expression of the TVA receptor and rabies glycoprotein (G) were unilaterally injected into the basolateral amygdala of PV-IRES-Cre mice, restricting subsequent infection of G-deleted rabies virus (RV*d*G) pseudotyped with the envelop protein A (EnvA) to PV-INs and their retrograde monosynaptic contacts (Figure 5A). In addition to other subcortical and cortical regions (Figure S5), amygdala PV-INs received robust innervation from the medial geniculate nucleus (MGN) and the temporal association cortex (TeA) (Figures 5B and 5C). These regions are known to convey auditory input to amygdala, and their axon terminals are presumed to be involved in plasticity of internal and external capsule synaptic responses in amygdala excitatory neurons (LeDoux, 2000).

To investigate functional synaptic connectivity between MGN/TeA and amygdala PV-INs, we targeted these areas with injections of an AAV encoding eYFP-tagged channelrhodopsin 2 (ChR2-eYFP) driven by the CaMKII promoter in PV-IRES-Cre:Ai9 double transgenic mice, in which tdTomato expression is localized to PV-INs. Following these injections, eYFP+ terminals were observed in the basolateral amygdala complex. However, MGN terminals were largely restricted to LA, whereas TeA terminals could be observed in both LA and BA (Figures 5D and 5E). Terminal stimulation evoked polysynaptic EPSCs in PV-INs (Figure 5F), likely the result of strong local excitatory connections to PV-INs. To isolate monosynaptic currents, we blocked NMDA receptors with saturating CPP (10 μM) and AMPA receptors with subsaturating CNQX (1 μM). Resulting optic-evoked EPSCs (oEPSCs) could be completely abolished with saturating CNQX (10 μM; Figure 5F). Consistent with anatomical labeling, blue-light stimulation of MGN terminals resulted in monosynaptic oEPSCs in the vast majority of LA PV-INs (36/41), but no responses were detected in BA PV-INs (0/10). In contrast, oEPSCs were observed in both LA (28/35) and BA (27/30) PV-INs during TeA terminal stimulation (Figure 5G). Onset latencies of oEPSCs were consistent with monosynaptic transmission (Figure 5H).

We next measured PPR of oEPSCs to determine whether MGN and TeA afferent plasticity could account for learning-dependent changes in glutamate release (Figure 4). Surprisingly, this revealed no effect of fear conditioning on PPR at MGN synapses onto LA PV-INs (Figures 5I and 5J). However, consistent with the results of electrical stimulation (Figures 4D–4I), PPR of TeA oEPSCs was increased in paired animals relative to both naive and unpaired controls in LA (repeated-measures ANOVA, main effect of group, $F_{(2,72)} = 12.03$, $p = 0.0002$) but not BA PV-INs (Figures 5K–5N). These data confirm the nucleus specificity of PV-IN afferent plasticity in the auditory cortical pathway but suggest that plasticity of internal capsule responses is not attributable to auditory thalamic inputs.

Nucleus- and Synapse-Specific Reduction of GABA Release from PV-INs

Previous studies suggest that changes in inhibitory transmission may occur after fear conditioning, but this work relied mainly on analysis of GABA receptors from amygdala lysates (Chhatwal et al., 2005; Heldt and Ressler, 2007; Lin et al., 2011). It therefore remains unclear whether fear encoding alters GABA transmission within specific microcircuits. To enable stimulation of synapses formed by PV-INs, we injected Cre-inducible AAV vectors encoding ChR2-eYFP into PV-IRES-Cre mice, resulting in somal and axonal eYFP expression in PV-INs (Figures 6A and 6B) and blue-light-driven action potential generation (Figure 6C). Consistent with selective recombination in PV-INs (Figures 1A and S1), we verified that optic stimulation in these mice did not result in non-GABAergic transmission (Figures 6D–6F). Nevertheless, subsequent experiments were conducted in the presence of glutamate receptor antagonists. We used paired-pulse optic stimulation ($\lambda = 470$ nm) to determine whether fear conditioning leads to changes in GABA release from PV-INs onto neighboring principal neurons. Repeated-measures ANOVA revealed that PPR differed between conditions in the LA (repeated-measures ANOVA, main effect of group, $F_{(2,68)} = 26.13$, $p < 0.001$) but not in the BA. In LA, PPR was increased in paired, but not unpaired, animals relative to naive controls. This decrease in GABA release was at least partly specific to PV-IN inputs because IPSCs evoked by local field stimulation were not modulated by training (Figures S6A–S6C).

To determine whether PV-IN-specific plasticity corresponds to an overall reduction of inhibition onto LA principal neurons, we collected spontaneous IPSCs (sIPSCs) from these cells after fear conditioning. Consistent with a previous report (Lin et al., 2011), both sIPSC frequency (one-way ANOVA, $F(2,51) = 11.17$, $p = 0.0001$) and amplitude (one-way ANOVA, $F(2,51) = 6.80$, $p = 0.003$) was decreased in LA of animals that received paired training (Figures S6D–S6G). However, no changes in sIPSC properties were observed in BA principal neurons (Figures S6H–S6K). While our data suggest that decreased GABA release from PV-INs may contribute to reduced sIPSC frequency in LA, it is important to consider that these events reflect the cumulative action of GABA transmission not only from PV-INs but also from other inhibitory cell types.

Given the dense innervation of PV-INs by other PV-INs in the BA (Muller et al., 2005; Woodruff and Sah, 2007), we next questioned whether the observed changes in GABA release are specific to glutamatergic targets, in particular because fear conditioning altered mIPSC frequency in BA PV-INs (Figure 3L). To facilitate fluorescence-based targeting of PV-INs without activating ChR2, we injected Cre-dependent AAV-ChR2 into the amygdala of PV-IRES-Cre:Ai9 double transgenic mice (Figure 6K). This strategy allowed us to use non-overlapping LED spectra for PV-IN visualization and ChR2 excitation (Figure 6L). PPR analysis of PV-IN→PV-IN oIPSCs revealed no learning-induced differences in GABA release in LA or BA (Figures 6M–6P), indicating that, in

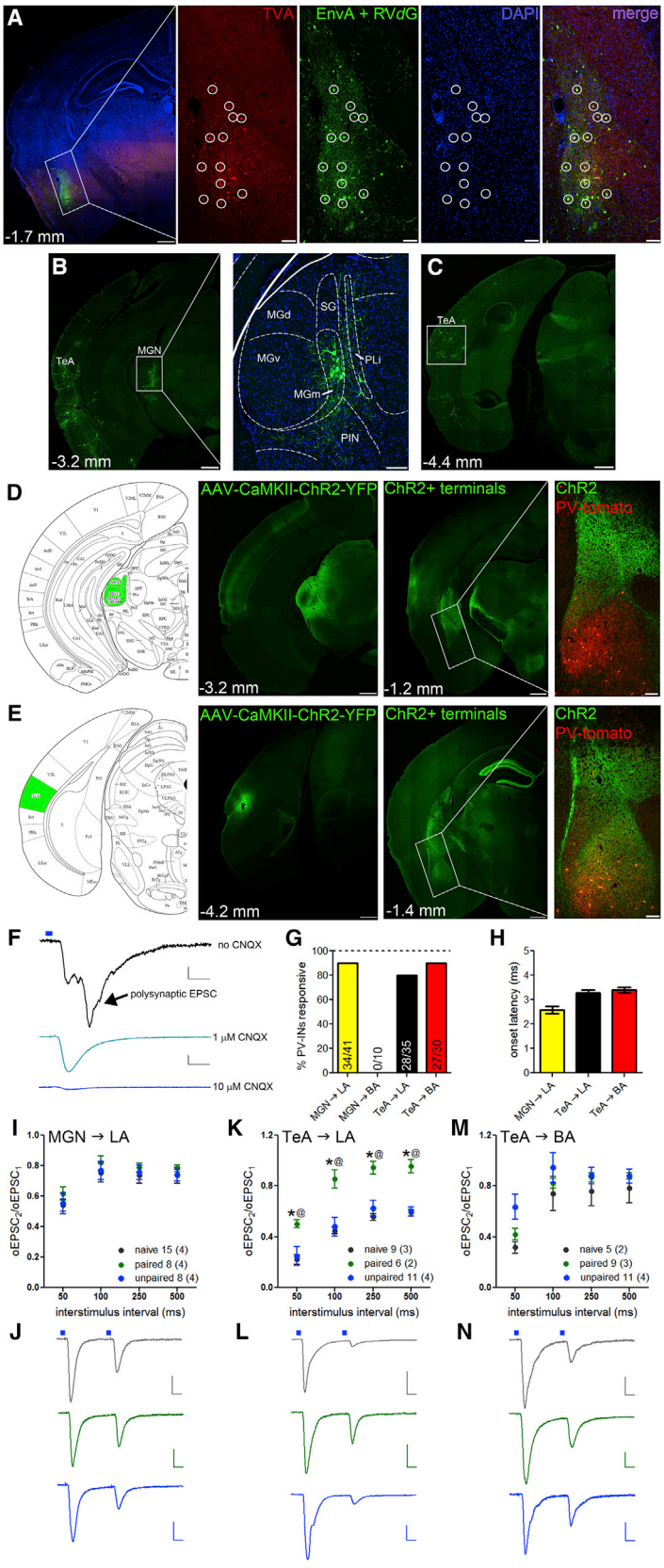

Figure 5. Presynaptic Origins of Internal and External Capsule Plasticity

(A) AAV-FLEX-TVA-mCherry and AAV-FLEX-RG (rabies glycoprotein) was unilaterally injected into the basolateral amygdala of PV-IRES-Cre mice to restrict subsequent expression of EnvA+RV*d*G-eGFP to PV-INs and their monosynaptic retrograde partners. Confocal images of the injection site (boxed portion on left) are enlarged in the right panels. Retrograde labeling only occurred from PV-INs that coexpressed mCherry (red) and eGFP (green; circles). Scales: low magnification, 500 μm; enlargements, 100 μm.

(B and C) eGFP-positive cell bodies were observed in temporal association cortex (TeA; [B], [C]) and the medial portion of the medial geniculate nucleus (MGN; [B]). The boxed portion of the MGN on left is enlarged in the center panel. MG dorsal (d), ventral (v), and medial (m); suprageniculate nucleus (SG); posterior limitans nucleus (PLi); posterior intralaminar nucleus (PIN). Scales: low magnification, 500 μm; enlargement, 100 μm.

(D and E) AAV-CaMKII-ChR2-eYFP was injected into the MGN (D) and TeA (E) of PV-IRES-Cre mice crossed to ROSA-tdTomato reporter mice to target PV-INs for electrophysiological recordings without exciting ChR2. eYFP-positive terminal expression is shown in center panels with the boxed portion representing the enlarged images of basolateral amygdala to the right. Scales: low magnification, 500 μm; enlargements, 100 μm.

(F) Optic-evoked EPSCs (oEPSCs) were conducted in the presence of 10 μM CPP and 1 μM CNQX to prevent polysynaptic activity and isolate monosynaptic currents. oEPSCs were abolished by saturating CNQX (10 μM). Scales: 10 pA × 10 ms.

(G) Terminal stimulation elicited oEPSCs from both pathways onto LA PV-INs; only TeA oEPSCs were observed in BA PV-INs.

(H) Onset latency of oEPSCs was consistent with monosynaptic transmission in both pathways.

(I–J) Fear learning did not alter PPR of oEPSCs at MGN→LA PV-IN synapses. Representative traces in (J).

(K–N) PPR of oEPSCs at TeA→PV-IN synapses was increased in paired compared to unpaired and naive mice in LA ([K], representative traces in [L]) but not BA ([M], representative traces in [N]).

(J, L, and N) Representative traces shown at the 50 ms interstimulus interval. Scales ([J], [L], [N]): 10 pA × 50 ms.

(I, K, and M) Repeated-measures ANOVA followed by Holm-Bonferroni. n/group indicated on graphs. Data presented as mean ± SEM.

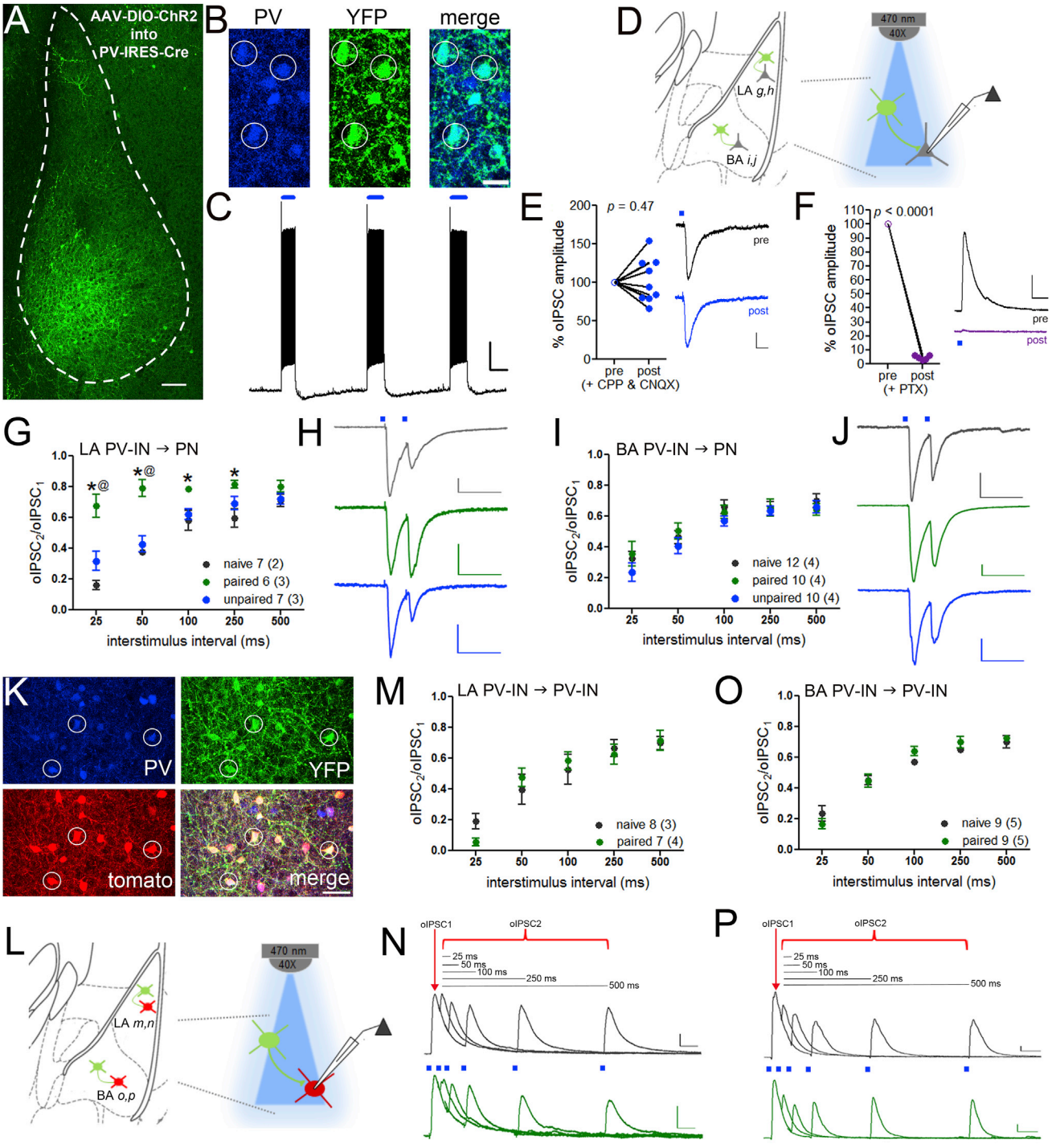

Figure 6. Nucleus- and Target-Specific Reduction in GABA Release from PV-INs after Auditory Fear Conditioning

(A) AAV-DIO-ChR2-eYFP was injected into the basolateral amygdala of PV-IRES-Cre mice for optogenetic-assisted in vitro slice electrophysiology. Scale: 100 μm.

(B) Immunofluorescence staining confirmed that eYFP (green) was exclusively expressed in PV-positive neurons (blue). Scale: 25 μm.

(C) Blue light (λ = 470 nm) evoked action potential generation in ChR2+ PV-INs. Scale: 15 mV × 1 s.

(D) Recording configuration in (E)–(J). Release probability at PV-IN→principal neuron (PN) synapses was assayed by paired-pulse optic stimulation (λ = 470 nm) in LA ([G], [H]) and BA ([I], [J]).

(E and F) Light-evoked currents were unaffected by the glutamate receptor antagonists APV and CNQX ([E], scale: 20 pA × 25 ms) and abolished by the $GABA_A$ receptor antagonist PTX ([F], scale: 100 pA × 50 ms). Data are normalized to pre-antagonist amplitudes.

(legend continued on next page)

addition to being nucleus-specific, learning-dependent changes in PV-IN inhibition exhibit target selectivity.

A previous report found that fear conditioning induces alterations in GABA receptor expression in the lateral amygdala that are reversible by extinction (Lin et al., 2011). Therefore, we postulated that GABA release properties might exhibit similar bidirectional regulation. However, increased PPR of PV-IN IPSCs was not reversed by extinction training (Figure S7).

Intrinsic Excitability of Basolateral Amygdala PV-INs Is Unaltered by Fear Memory Encoding

While synapse-selective changes can alter the relationship of PV-INs to specific presynaptic and postsynaptic targets, firing rate plasticity could render PV-INs more or less excitable and thus impact their general integration. To evaluate this possibility, we examined action potential discharge in PV-INs in response to somatic current injections after fear conditioning. No experience-dependent differences in firing frequency were observed in LA or BA (Figures 7A–7F). In naive animals, however, PV-INs in BA were more excitable than those in LA (Figure 7G), exhibiting reduced rheobase current (independent samples t test, $t_{(23)}$ = 2.19, p = 0.04) and increased firing frequency (repeated-measure ANOVA, main effect of nucleus, $F_{(1,\ 207)}$ = 17.81, p = 0.0003). This nucleus-specific difference is likely attributable to increased cell size, as inferred from a difference in online capacitance measurements from PV-INs (LA 103.00 ± 32.48 pF; BA 69.17 ± 24.13 pF; independent-samples t test, $t_{(30)}$ = 3.12, p = 0.004). No other differences in passive membrane properties were observed. Likewise, no differences were observed in individual spike characteristics (including threshold, amplitude, duration, or afterhyperpolization; Figures 7H–7K).

DISCUSSION

With the aid of cell-selective reporters and optogenetic tools, we achieved several novel insights into amygdala PV-IN function. First, the amygdala is populated by two distinct networks of PV-INs defined by their nucleus location, dendritic complexity, and potency of afferent excitation. Second, these striking differences correlate with the preferential engagement of LA, but not BA, PV-INs in afferent-evoked feedforward inhibition. Third, fear memory encoding results in selective functional downregulation of LA PV-IN microcircuitry through plasticity of both afferent input as well as GABA release. Importantly, input plasticity could be localized in part to projections from TeA, an auditory cortical region that displays increased CS-related activity after fear acquisition (Quirk et al., 1997). Together, our studies point to multimodal plasticity of discrete PV-IN microcircuits as potentially integral to aversive memory encoding. Decreased PV-IN activity would be expected to enhance recruitment of amygdala excitatory projection neurons and corresponding fear-related behaviors by sensory stimulation.

Several recent studies indicate that feedforward engagement of PV-INs in the cortex is pathway-specific (Delevich et al., 2015; Lee et al., 2014; Li et al., 2014; Rock and Apicella, 2015; Yang et al., 2013). Here we show that such differential recruitment also occurs among amygdala PV-IN subpopulations within the same afferent pathway and is correlated with PV-IN morphological and physiological specialization. A likely explanation for increased excitatory drive in LA PV-INs is that they possess more dendritic compartments and a corresponding greater number of afferent synapses. On the other hand, the lack of feedforward inhibition from BA PV-INs is consistent with anatomical data suggesting that amygdala PV-INs are minimally targeted by cortical afferents (Smith et al., 2000), even though our results establish that the majority of BA PV-INs can be driven by cortical stimulation. However, this and other studies have largely focused on BA PV-INs, neglecting a comparatively sparse population of LA PV-INs that apparently compensate for their smaller numbers with greater excitatory drive. Indeed, while our viral injections led to eArch3.0 expression in an average of only two to four LA PV-INs per brain slice (Figure S2A), light-evoked suppression of these cells was surprisingly effective at reducing feedforward inhibition. Potent recruitment of PV-INs by subcortical and cortical pathways may in part explain the relative silence of LA, compared to other amygdala nuclei, when sampled by in vivo electrodes (Gaudreau and Paré, 1996). Such properties also make PV-INs a potentially powerful substrate for experience-dependent gain modulation of amygdala input.

Past research has established an important role for excitatory synaptic strengthening within amygdala afferent pathways during the encoding of cued fear associations (Janak and Tye, 2015; Johansen et al., 2011; Nabavi et al., 2014). Although far less advanced, research into amygdala inhibitory transmission has suggested that memory encoding also alters GABAergic neuronal substrates (Chhatwal et al., 2005; Heldt and Ressler, 2007; Lin et al., 2011). Interestingly, whereas excitation and

(G) Paired pulse ratio (PPR) of PV-IN→PN IPSCs in LA was increased in mice that received paired training compared to unpaired and naive conditions. Representative traces in (H).

(I and J) PPRs were unaltered in BA (I). Representative traces in (J). Representative traces are shown at the 50 ms interstimulus interval. Scales: (H) 50 pA × 100 ms; (J) 60 pA × 100 ms.

(J) Representative traces. Representative traces are shown at the 50 ms interstimulus interval. Scales: (H) 50 pA × 100 ms; (J) 60 pA × 100 ms.

(K) AAV-DIO-ChR2-eYFP was injected into the basolateral amygdala of PV-IRES-Cre mice crossed to ROSA-tdTomato reporter mice to target PV-INs for electrophysiological recordings without gating ChR2. Scale: 50 μm.

(L) Schematic of (M)—(P). Release probability at PV-IN→PV-IN synapses was assayed by paired-pulse optical stimulation (λ = 470 nm) during recording from tdTomato-positive PV-INs in LA ([M], [N]) and BA ([O], [P]).

(M–P) PPR of PV-IN→PV-IN IPSCs was unaffected by training in the LA ([M], representative traces in [N]) and BA ([O], representative traces in [P]). IPSC recordings were conducted at 0 mV in order to exclude postsynaptic ChR2 currents based on their ionic reversal. Scales: ([N], [P]) 50 pA × 50 ms.

(E and F) Paired samples t test.

(G, I, M, and O) n/group indicated in graphs. Repeated-measures ANOVA followed by planned comparisons with Holm-Bonferroni. *p < 0.05 naive versus paired, @ p < 0.05 paired versus unpaired. Data presented as mean ± SEM.

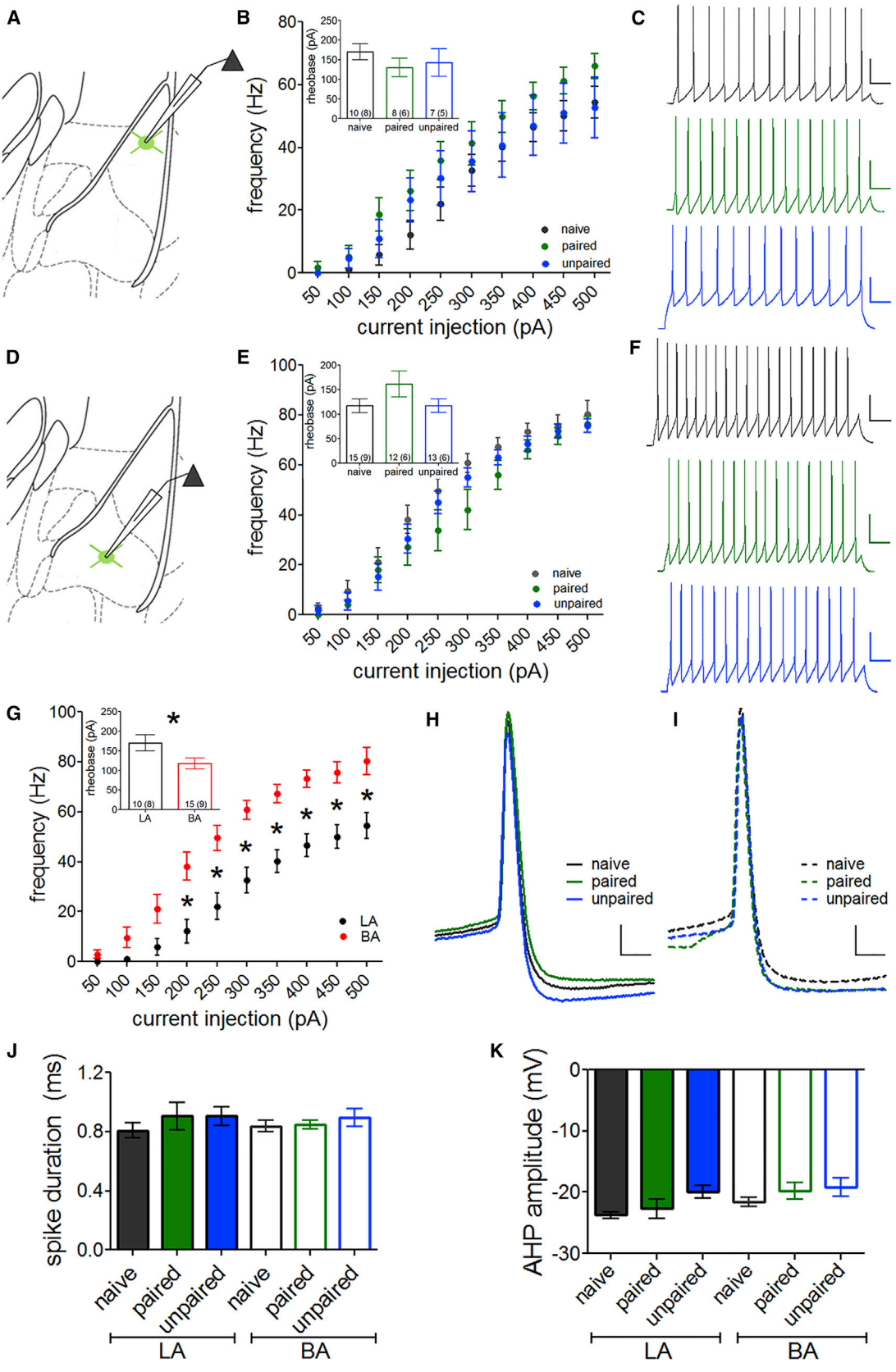

(legend on next page)

inhibition are co-upregulated in ex vivo preparations during the expression of long-term potentiation (Lamsa et al., 2005), our work indicates that glutamatergic (Arruda-Carvalho and Clem, 2014; Clem and Huganir, 2010, 2013) and GABAergic function (present study) are modified in opposite directions following emotional learning. In contrast to excitatory neuronal plasticity, which involves presynaptic and postsynaptic alterations as well as changes in membrane excitability (Johansen et al., 2011; Sigurdsson et al., 2007), PV-IN plasticity was localized to presynaptic compartments. Similar to our findings, a recent study reported that intercalated GABAergic projection neurons that surround the basolateral amygdala display decreased glutamatergic responses following fear conditioning (Asede et al., 2015). To our knowledge, however, ours is the first study to describe plasticity of GABA release following associative learning. Since target-selective structural plasticity has been observed in PV-INs after extinction training (Trouche et al., 2013), it seems that dynamic regulation of PV-IN terminals could be a fundamental mechanism of emotional learning. However, we did not observe reversal of decreased GABA release onto principal neurons after extinction learning (Figure S7), indicating different modes of experience-dependent plasticity may govern the role of amygdala PV-INs in fear conditioning and extinction.

The mechanisms mediating decreased transmission from PV-INs after fear learning are currently unknown. Upregulation of both parvalbumin and glutamic acid decarboxylase 67 (GAD67, a GABA synthetic enzyme) in PV-INs has been proposed to be a signature of memory encoding across multiple paradigms and brain regions, including in the hippocampus after contextual fear conditioning (Donato et al., 2013). These changes would be predicted to decrease PPR of oIPSCs due to increased GABA stores as well as enhanced calcium buffering capacity of PV-INs (Caillard et al., 2000). However, our data show that these findings may not extrapolate to the amygdala, where fear conditioning leads to a decrease in PPR of PV-IN-mediated oIPSCs.

On the other hand, recently described effects of neuromodulators on PV-IN release properties suggest their potential involvement in fear-related inhibitory plasticity. Dopaminergic terminals form dense perisomatic synapses onto amygdala PV-INs (Brinley-Reed and McDonald, 1999; Pinard et al., 2008), and ex vivo dopamine application acts through D2 receptors to reduce GABA release from PV-INs (Chu et al., 2012). Similar to fear conditioning (Figure 6), dopamine effects are manifested at PV-IN synapses onto principal cells but not interneurons. In addition, D2 receptor activation reduces the frequency of sIPSCs as well as the magnitude of principal neuron feedforward inhibition in LA (Bissière et al., 2003). Thus, dopamine release may be a key mechanism leading to PV-IN plasticity and corresponding amygdala disinhibition.

An intriguing outcome of our optogenetic interrogations was that MGN terminals did not exhibit changes in glutamate release onto PV-INs following fear conditioning (Figure 5), as predicted based on electrical stimulation of the internal capsule (Figures 4A–4C), in which MGN axons could be detected based on eYFP fluorescence. It seems unlikely that thalamic expression of ChR2 prevented or occluded plasticity, since changes in PPR were readily observed at TeA synapses. Therefore, we suggest that internal capsule stimulation recruits other subcortical projections whose modification may be important for auditory fear conditioning. Future experiments should examine whether these projections also account for previously described plasticity of internal capsule EPSCs in principal neurons (Clem and Huganir, 2010, 2013; McKernan and Shinnick-Gallagher, 1997; Namburi et al., 2015; Rumpel et al., 2005; Tye et al., 2008; Zhou et al., 2009), a finding that would upend the conventional wisdom that excitatory synaptic strengthening is attributable to the auditory thalamic pathway. It is worth noting, however, that even though MGN synapses were unaffected by training, feedforward inhibition from this pathway could nevertheless be modulated by decreased output of PV-INs (Figure 6).

Another important unanswered question is which neuronal population(s) are responsible for enhanced inhibition onto PV-INs in BA after fear learning (Figure 3L). While PV-INs are densely interconnected in this region (Muller et al., 2005; Woodruff and Sah, 2007), GABA release at PV-IN→PV-IN synapses was not modulated by fear encoding (Figure 6), indicating that another GABAergic population is responsible for this effect. Although recordings from sensory cortex point to somatostatin-containing interneurons as major regulators of PV-INs (Pfeffer et al., 2013; Xu et al., 2013), only a very small percentage of somatostatin-positive terminals form synapses with PV-INs in amygdala (Muller et al., 2007). However, the GABAergic cells that mediate inhibitory plasticity are not necessarily intrinsic to the amygdala and may be connected to PV-INs through long-range projections, such as those arising from the basal forebrain that densely and selectively terminate onto PV-INs in the BA but not LA (McDonald et al., 2011). Future studies will be required examine the contributions of intrinsic and extrinsic GABAergic populations to experience-dependent plasticity in amygdala PV-IN microcircuits.

Figure 7. Fear Memory Encoding Does Not Affect PV-IN Intrinsic Excitability

Action potentials were elicited in PV-INs in LA ([A]–[C]) and BA ([D]–[F]) by somatic current injections of increasing amplitude.

(A) Recording configuration in (B) and (C).

(B and C) No differences in intrinsic excitability were observed among groups in LA PV-INs ([B], representative traces at the 200 pA current injection in [C]).

(D) Recording configuration in (E) and (F).

(E and F) No differences in intrinsic excitability were observed among groups in BA PV-INs ([E], representative traces at the 200 pA current injection in [F]). Scales: 50 pA × 25 ms.

(G) In naive animals, PV-INs in LA were less excitable than PV-INs in BA, requiring more current to fire a single action potential (rheobase current; inset) and firing fewer action potentials to current injections greater than 150 pA.

(H–K) Individual spike characteristics were quantified in LA (H) and BA (I) at rheobase. Overlays of representative traces are shown. Scales: 10 pA × 2 ms. No differences were observed among groups or between nuclei in any spike parameter, including spike duration (J) and afterhyperpolarization (AHP) amplitude (K). n/group indicated on graphs.

(G) Repeated-measures ANOVA followed by Holm-Bonferroni or independent samples t test (inset). *$p < 0.05$. Data presented as mean ± SEM.

Regarding the outcomes of real-life traumatic experiences, the various forms of PV-IN-specific plasticity that we describe could contribute to amygdala hyperexcitability as well as generalization of conditioned fear to nonspecific stimuli, which in certain cases may serve an evolutionarily adaptive purpose. However, such plasticity may also be a precipitating factor for escalating fear and anxiety in PTSD. Indeed, preclinical animal models suggest that PV-IN dysfunction may be involved in pathological, extinction-resistant fear (Bissonette et al., 2014; Brown et al., 2015; Lucas et al., 2014). Therefore, experiments should examine whether chronic stress or trauma is associated with altered inhibitory plasticity and whether these effects may underlie progression to emotional dysfunction. Our results provide an initial framework for elucidating these roles by clarifying the basic function of PV-IN microcircuits and their modification by aversive conditioning.

EXPERIMENTAL PROCEDURES

Further details can be found in the Supplemental Experimental Procedures.

Animals

All experiments were approved in advance by the Institutional Care and Use Committee of the Icahn School of Medicine at Mount Sinai. Experiments were conducted on male mice 28–40 days of age from the following lines: C56Bl/6J (RRID: IMSR_JAX:000664), PV-IRES-Cre (RRID: IMSR_JAX:008069), R26-STOP-eYFP (RRID: IMSR_JAX:006148), and Rosa-CAG-LSL-tdTomato-WPRE (Ai9; RRID: IMSR_JAX:007909).

Viral Targeting for Electrophysiology

Viral constructs were purchased from the University of Pennsylvania Vector Core and included AAV1-EF1a-DIO-hChR2(H134R)-eYFP-WPRE (Addgene #20298), AAV1-CBA-Flex-Arch-GFP (Addgene #22222), and AAV1-CamKIIa-hChR2(H134R)-eYFP-WPRE (Addgene #26969P). Viral constructs (0.3–1 μl) were bilaterally injected into the basolateral amygdala (AP −1.4, ML ± 3.3, DV −5.0), temporal association cortex (AP −4.0, ML ± 4.0, DV −3.5), and medial geniculate nucleus (AP −3.2, ML ± 1.8, DV −3.5).

Viral Targeting for Monosynaptic Circuit Tracing

Viral constructs were purchased from the University of North Carolina Vector Core (AAV8-EF1a-FLEX-TVA-mCherry, Addgene #38044; AAV8-CA-FLEX-RG, Addgene #38043; Watabe-Uchida et al., 2012) and the Salk Institute Gene Transfer, Targeting, and Therapeutics Core (EnvA G-deleted Rabies-eGFP, Addgene #32635; Wickersham et al., 2007). Unilateral basolateral amygdala injections of AAV8-EF1a-FLEX-TVA-mCherry and AAV8-CA-FLEX-RG (1:1 ratio) were conducted 3 weeks prior to EnvA G-deleted Rabies-eGFP, and animals were sacrificed by transcardial perfusion 1 week later.

Immunofluorescence Staining

Immunofluoresence was conducted as previously described (Lucas et al., 2014).

Fear Conditioning

Cued auditory fear conditioning was conducted in sound attenuating chambers with automated stimulus delivery software (MedAssociates) as previously described (Clem and Huganir, 2010, 2013).

Slice Electrophysiology

Acute coronal slices of the basolateral amygdala were prepared as previously described (Clem and Huganir, 2010, 2013). Cells were visualized on an upright DIC microscope equipped with objective-coupled LEDs (460 nm and broad spectrum [white]; Prizmatix, Givat-Shmuel, Israel) for the identification of fluorescence-labeled cells as well as optogenetic cellular manipulations. Data were low-pass filtered at 3 kHz (evoked) and 10 kHz (spontaneous, miniature) and acquired at 10 kHz using Multiclamp 700B and pClamp 10 (Molecular Devices). Evoked data were analyzed in Clampfit 10 (Molecular Devices); spontaneous and miniature currents were analyzed with MiniAnalysis (Synaptosoft). All data analyses were conducted blind to the experimental group.

Morphological Analysis

Live brain sections were prepared as for slice electrophysiology. PV-INs were identified by tdTomato expression, patched, and filled with 0.5% biocytin. Tissue preparation and morphological analyses were conducted as previously described (Dougherty et al., 2014).

Statistics

Two-tail paired t tests (one group), two-tail independent samples t tests (two groups), one-way ANOVA ($\geq$3 groups), two-way ANOVA ($\geq$2 groups with $\geq$ 2 variables), or two-way repeated-measures ANOVA ($\geq$2 groups with repeating variable) were implemented to determine statistical significance. All post hoc tests were chosen to maintain family wise error rate at 0.05. Data are presented as mean ± SEM with *n* as the number of cells followed by the number of animals in parentheses.

SUPPLEMENTAL INFORMATION

Supplemental Information includes seven figures and Supplemental Experimental Procedures and can be found with this article online at http://dx.doi.org/10.1016/j.neuron.2016.06.032.

AUTHOR CONTRIBUTIONS

Conceptualization, E.K.L. and R.L.C.; Methodology, E.K.L. and R.L.C.; Investigation, E.K.L., A.M.J., and R.L.C.; Writing – Original Draft, E.K.L. and R.L.C.; Writing – Review & Editing, E.K.L., A.M.J., H.M., and R.L.C.; Funding Acquisition, E.K.L. and R.L.C.; Resources, H.M. and R.L.C.; Supervision, E.K.L. and R.L.C.

ACKNOWLEDGMENTS

This work was funded by NIH grants MH105414 (R.L.C.), EY026053 (H.M.), and MH096678 (E.K.L.); a NARSAD Young Investigator Award (R.L.C.); and seed funds from the Friedman Brain Institute at the Icahn School of Medicine at Mount Sinai. We would like to thank Timothy Rumbell for instruction on spike analysis, Dara Dickstein and Katina Calakos for assistance with morphological analysis; Elisa Nabel for guidance on Cre-dependent monosynaptic input mapping; Stephen Salton for sharing his equipment; and Karl Deisseroth, Ed Boyden, Ed Callaway, and Naoshige Uchida for their generous contribution of viral vectors. The authors declare no conflicts of interest.

Received: August 17, 2015
Revised: May 12, 2016
Accepted: June 15, 2016
Published: July 14, 2016

REFERENCES

Arruda-Carvalho, M., and Clem, R.L. (2014). Pathway-selective adjustment of prefrontal-amygdala transmission during fear encoding. J. Neurosci. *34*, 15601–15609.

Asede, D., Bosch, D., Lüthi, A., Ferraguti, F., and Ehrlich, I. (2015). Sensory inputs to intercalated cells provide fear-learning modulated inhibition to the basolateral amygdala. Neuron *86*, 541–554.

Bauer, E.P., and LeDoux, J.E. (2004). Heterosynaptic long-term potentiation of inhibitory interneurons in the lateral amygdala. J. Neurosci. *24*, 9507–9512.

Bienvenu, T.C., Busti, D., Magill, P.J., Ferraguti, F., and Capogna, M. (2012). Cell-type-specific recruitment of amygdala interneurons to hippocampal theta rhythm and noxious stimuli in vivo. Neuron *74*, 1059–1074.

Bissière, S., Humeau, Y., and Lüthi, A. (2003). Dopamine gates LTP induction in lateral amygdala by suppressing feedforward inhibition. Nat. Neurosci. *6*, 587–592.

Bissonette, G.B., Bae, M.H., Suresh, T., Jaffe, D.E., and Powell, E.M. (2014). Prefrontal cognitive deficits in mice with altered cerebral cortical GABAergic interneurons. Behav. Brain Res. *259*, 143–151.

Bremner, J.D., Innis, R.B., Southwick, S.M., Staib, L., Zoghbi, S., and Charney, D.S. (2000). Decreased benzodiazepine receptor binding in prefrontal cortex in combat-related posttraumatic stress disorder. Am. J. Psychiatry *157*, 1120–1126.

Brinley-Reed, M., and McDonald, A.J. (1999). Evidence that dopaminergic axons provide a dense innervation of specific neuronal subpopulations in the rat basolateral amygdala. Brain Res. *850*, 127–135.

Brown, J.A., Ramikie, T.S., Schmidt, M.J., Báldi, R., Garbett, K., Everheart, M.G., Warren, L.E., Gellért, L., Horváth, S., Patel, S., and Mirnics, K. (2015). Inhibition of parvalbumin-expressing interneurons results in complex behavioral changes. Mol. Psychiatry *20*, 1499–1507.

Caillard, O., Moreno, H., Schwaller, B., Llano, I., Celio, M.R., and Marty, A. (2000). Role of the calcium-binding protein parvalbumin in short-term synaptic plasticity. Proc. Natl. Acad. Sci. USA *97*, 13372–13377.

Chhatwal, J.P., Myers, K.M., Ressler, K.J., and Davis, M. (2005). Regulation of gephyrin and GABAA receptor binding within the amygdala after fear acquisition and extinction. J. Neurosci. *25*, 502–506.

Chow, B.Y., Han, X., Dobry, A.S., Qian, X., Chuong, A.S., Li, M., Henninger, M.A., Belfort, G.M., Lin, Y., Monahan, P.E., and Boyden, E.S. (2010). High-performance genetically targetable optical neural silencing by light-driven proton pumps. Nature *463*, 98–102.

Chu, H.Y., Ito, W., Li, J., and Morozov, A. (2012). Target-specific suppression of GABA release from parvalbumin interneurons in the basolateral amygdala by dopamine. J. Neurosci. *32*, 14815–14820.

Clem, R.L., and Huganir, R.L. (2010). Calcium-permeable AMPA receptor dynamics mediate fear memory erasure. Science *330*, 1108–1112.

Clem, R.L., and Huganir, R.L. (2013). Norepinephrine enhances a discrete form of long-term depression during fear memory storage. J. Neurosci. *33*, 11825–11832.

Courtin, J., Chaudun, F., Rozeske, R.R., Karalis, N., Gonzalez-Campo, C., Wurtz, H., Abdi, A., Baufreton, J., Bienvenu, T.C., and Herry, C. (2014). Prefrontal parvalbumin interneurons shape neuronal activity to drive fear expression. Nature *505*, 92–96.

Delevich, K., Tucciarone, J., Huang, Z.J., and Li, B. (2015). The mediodorsal thalamus drives feedforward inhibition in the anterior cingulate cortex via parvalbumin interneurons. J. Neurosci. *35*, 5743–5753.

Donato, F., Rompani, S.B., and Caroni, P. (2013). Parvalbumin-expressing basket-cell network plasticity induced by experience regulates adult learning. Nature *504*, 272–276.

Dorrn, A.L., Yuan, K., Barker, A.J., Schreiner, C.E., and Froemke, R.C. (2010). Developmental sensory experience balances cortical excitation and inhibition. Nature *465*, 932–936.

Dougherty, S.E., Bartley, A.F., Lucas, E.K., Hablitz, J.J., Dobrunz, L.E., and Cowell, R.M. (2014). Mice lacking the transcriptional coactivator PGC-1α exhibit alterations in inhibitory synaptic transmission in the motor cortex. Neuroscience *271*, 137–148.

Feusner, J., Ritchie, T., Lawford, B., Young, R.M., Kann, B., and Noble, E.P. (2001). GABA(A) receptor beta 3 subunit gene and psychiatric morbidity in a post-traumatic stress disorder population. Psychiatry Res. *104*, 109–117.

Gaudreau, H., and Paré, D. (1996). Projection neurons of the lateral amygdaloid nucleus are virtually silent throughout the sleep–waking cycle. J. Neurophysiol. *75*, 1301–1305.

Geuze, E., van Berckel, B.N., Lammertsma, A.A., Boellaard, R., de Kloet, C.S., Vermetten, E., and Westenberg, H.G. (2008). Reduced GABAA benzodiazepine receptor binding in veterans with post-traumatic stress disorder. Mol. Psychiatry *13*, 74–83.

Heldt, S.A., and Ressler, K.J. (2007). Training-induced changes in the expression of GABAA-associated genes in the amygdala after the acquisition and extinction of Pavlovian fear. Eur. J. Neurosci. *26*, 3631–3644.

House, D.R., Elstrott, J., Koh, E., Chung, J., and Feldman, D.E. (2011). Parallel regulation of feedforward inhibition and excitation during whisker map plasticity. Neuron *72*, 819–831.

Hu, H., Gan, J., and Jonas, P. (2014). Interneurons. Fast-spiking, parvalbumin^{+} GABAergic interneurons: from cellular design to microcircuit function. Science *345*, 1255263.

Janak, P.H., and Tye, K.M. (2015). From circuits to behaviour in the amygdala. Nature *517*, 284–292.

Johansen, J.P., Cain, C.K., Ostroff, L.E., and LeDoux, J.E. (2011). Molecular mechanisms of fear learning and memory. Cell *147*, 509–524.

Katagiri, H., Fagiolini, M., and Hensch, T.K. (2007). Optimization of somatic inhibition at critical period onset in mouse visual cortex. Neuron *53*, 805–812.

Lamsa, K., Heeroma, J.H., and Kullmann, D.M. (2005). Hebbian LTP in feedforward inhibitory interneurons and the temporal fidelity of input discrimination. Nat. Neurosci. *8*, 916–924.

LeDoux, J.E. (2000). Emotion circuits in the brain. Annu. Rev. Neurosci. *23*, 155–184.

Lee, A.T., Gee, S.M., Vogt, D., Patel, T., Rubenstein, J.L., and Sohal, V.S. (2014). Pyramidal neurons in prefrontal cortex receive subtype-specific forms of excitation and inhibition. Neuron *81*, 61–68.

Letzkus, J.J., Wolff, S.B., Meyer, E.M., Tovote, P., Courtin, J., Herry, C., and Lüthi, A. (2011). A disinhibitory microcircuit for associative fear learning in the auditory cortex. Nature *480*, 331–335.

Li, L.Y., Ji, X.Y., Liang, F., Li, Y.T., Xiao, Z., Tao, H.W., and Zhang, L.I. (2014). A feedforward inhibitory circuit mediates lateral refinement of sensory representation in upper layer 2/3 of mouse primary auditory cortex. J. Neurosci. *34*, 13670–13683.

Lin, H.C., Tseng, Y.C., Mao, S.C., Chen, P.S., and Gean, P.W. (2011). GABAA receptor endocytosis in the basolateral amygdala is critical to the reinstatement of fear memory measured by fear-potentiated startle. J. Neurosci. *31*, 8851–8861.

Lucas, E.K., Jegarl, A., and Clem, R.L. (2014). Mice lacking TrkB in parvalbumin-positive cells exhibit sexually dimorphic behavioral phenotypes. Behav. Brain Res. *274*, 219–225.

Mahan, A.L., and Ressler, K.J. (2012). Fear conditioning, synaptic plasticity and the amygdala: implications for posttraumatic stress disorder. Trends Neurosci. *35*, 24–35.

Mahanty, N.K., and Sah, P. (1998). Calcium-permeable AMPA receptors mediate long-term potentiation in interneurons in the amygdala. Nature *394*, 683–687.

McDonald, A.J., and Mascagni, F. (2001). Colocalization of calcium-binding proteins and GABA in neurons of the rat basolateral amygdala. Neuroscience *105*, 681–693.

McDonald, A.J., Muller, J.F., and Mascagni, F. (2011). Postsynaptic targets of GABAergic basal forebrain projections to the basolateral amygdala. Neuroscience *183*, 144–159.

McKernan, M.G., and Shinnick-Gallagher, P. (1997). Fear conditioning induces a lasting potentiation of synaptic currents in vitro. Nature *390*, 607–611.

Meyerhoff, D.J., Mon, A., Metzler, T., and Neylan, T.C. (2014). Cortical gamma-aminobutyric acid and glutamate in posttraumatic stress disorder and their relationships to self-reported sleep quality. Sleep *37*, 893–900.

Muller, J.F., Mascagni, F., and McDonald, A.J. (2005). Coupled networks of parvalbumin-immunoreactive interneurons in the rat basolateral amygdala. J. Neurosci. *25*, 7366–7376.

Muller, J.F., Mascagni, F., and McDonald, A.J. (2006). Pyramidal cells of the rat basolateral amygdala: synaptology and innervation by parvalbumin-immunoreactive interneurons. J. Comp. Neurol. *494*, 635–650.

Muller, J.F., Mascagni, F., and McDonald, A.J. (2007). Postsynaptic targets of somatostatin-containing interneurons in the rat basolateral amygdala. J. Comp. Neurol. *500*, 513–529.

Nabavi, S., Fox, R., Proulx, C.D., Lin, J.Y., Tsien, R.Y., and Malinow, R. (2014). Engineering a memory with LTD and LTP. Nature *511*, 348–352.

Namburi, P., Beyeler, A., Yorozu, S., Calhoon, G.G., Halbert, S.A., Wichmann, R., Holden, S.S., Mertens, K.L., Anahtar, M., Felix-Ortiz, A.C., et al. (2015). A circuit mechanism for differentiating positive and negative associations. Nature *520*, 675–678.

Pennington, D.L., Abé, C., Batki, S.L., and Meyerhoff, D.J. (2014). A preliminary examination of cortical neurotransmitter levels associated with heavy drinking in posttraumatic stress disorder. Psychiatry Res. *224*, 281–287.

Pfeffer, C.K., Xue, M., He, M., Huang, Z.J., and Scanziani, M. (2013). Inhibition of inhibition in visual cortex: the logic of connections between molecularly distinct interneurons. Nat. Neurosci. *16*, 1068–1076.

Pinard, C.R., Muller, J.F., Mascagni, F., and McDonald, A.J. (2008). Dopaminergic innervation of interneurons in the rat basolateral amygdala. Neuroscience *157*, 850–863.

Polepalli, J.S., Sullivan, R.K., Yanagawa, Y., and Sah, P. (2010). A specific class of interneuron mediates inhibitory plasticity in the lateral amygdala. J. Neurosci. *30*, 14619–14629.

Quirk, G.J., Armony, J.L., and LeDoux, J.E. (1997). Fear conditioning enhances different temporal components of tone-evoked spike trains in auditory cortex and lateral amygdala. Neuron *19*, 613–624.

Rock, C., and Apicella, A.J. (2015). Callosal projections drive neuronal-specific responses in the mouse auditory cortex. J. Neurosci. *35*, 6703–6713.

Rossi, S., De Capua, A., Tavanti, M., Calossi, S., Polizzotto, N.R., Mantovani, A., Falzarano, V., Bossini, L., Passero, S., Bartalini, S., and Ulivelli, M. (2009). Dysfunctions of cortical excitability in drug-naïve posttraumatic stress disorder patients. Biol. Psychiatry *66*, 54–61.

Rosso, I.M., Weiner, M.R., Crowley, D.J., Silveri, M.M., Rauch, S.L., and Jensen, J.E. (2014). Insula and anterior cingulate GABA levels in posttraumatic stress disorder: preliminary findings using magnetic resonance spectroscopy. Depress. Anxiety *31*, 115–123.

Rumpel, S., LeDoux, J., Zador, A., and Malinow, R. (2005). Postsynaptic receptor trafficking underlying a form of associative learning. Science *308*, 83–88.

Sah, P., Faber, E.S., Lopez De Armentia, M., and Power, J. (2003). The amygdaloid complex: anatomy and physiology. Physiol. Rev. *83*, 803–834.

Shin, R.M., Tsvetkov, E., and Bolshakov, V.Y. (2006). Spatiotemporal asymmetry of associative synaptic plasticity in fear conditioning pathways. Neuron *52*, 883–896.

Sigurdsson, T., Doyère, V., Cain, C.K., and LeDoux, J.E. (2007). Long-term potentiation in the amygdala: a cellular mechanism of fear learning and memory. Neuropharmacology *52*, 215–227.

Smith, Y., Paré, J.F., and Paré, D. (2000). Differential innervation of parvalbumin-immunoreactive interneurons of the basolateral amygdaloid complex by cortical and intrinsic inputs. J. Comp. Neurol. *416*, 496–508.

Szinyei, C., Heinbockel, T., Montagne, J., and Pape, H.C. (2000). Putative cortical and thalamic inputs elicit convergent excitation in a population of GABAergic interneurons of the lateral amygdala. J. Neurosci. *20*, 8909–8915.

Trouche, S., Sasaki, J.M., Tu, T., and Reijmers, L.G. (2013). Fear extinction causes target-specific remodeling of perisomatic inhibitory synapses. Neuron *80*, 1054–1065.

Turner, B.H., and Herkenham, M. (1991). Thalamoamygdaloid projections in the rat: a test of the amygdala's role in sensory processing. J. Comp. Neurol. *313*, 295–325.

Tye, K.M., Stuber, G.D., de Ridder, B., Bonci, A., and Janak, P.H. (2008). Rapid strengthening of thalamo-amygdala synapses mediates cue-reward learning. Nature *453*, 1253–1257.

Vaiva, G., Thomas, P., Ducrocq, F., Fontaine, M., Boss, V., Devos, P., Rascle, C., Cottencin, O., Brunet, A., Laffargue, P., and Goudemand, M. (2004). Low posttrauma GABA plasma levels as a predictive factor in the development of acute posttraumatic stress disorder. Biol. Psychiatry *55*, 250–254.

Vaiva, G., Boss, V., Ducrocq, F., Fontaine, M., Devos, P., Brunet, A., Laffargue, P., Goudemand, M., and Thomas, P. (2006). Relationship between posttrauma GABA plasma levels and PTSD at 1-year follow-up. Am. J. Psychiatry *163*, 1446–1448.

Vogels, T.P., Sprekeler, H., Zenke, F., Clopath, C., and Gerstner, W. (2011). Inhibitory plasticity balances excitation and inhibition in sensory pathways and memory networks. Science *334*, 1569–1573.

Watabe-Uchida, M., Zhu, L., Ogawa, S.K., Vamanrao, A., and Uchida, N. (2012). Whole-brain mapping of direct inputs to midbrain dopamine neurons. Neuron *74*, 858–873.

Wickersham, I.R., Lyon, D.C., Barnard, R.J., Mori, T., Finke, S., Conzelmann, K.K., Young, J.A., and Callaway, E.M. (2007). Monosynaptic restriction of transsynaptic tracing from single, genetically targeted neurons. Neuron *53*, 639–647.

Wolff, S.B., Gründemann, J., Tovote, P., Krabbe, S., Jacobson, G.A., Müller, C., Herry, C., Ehrlich, I., Friedrich, R.W., Letzkus, J.J., and Lüthi, A. (2014). Amygdala interneuron subtypes control fear learning through disinhibition. Nature *509*, 453–458.

Woodruff, A.R., and Sah, P. (2007). Networks of parvalbumin-positive interneurons in the basolateral amygdala. J. Neurosci. *27*, 553–563.

Xu, H., Jeong, H.Y., Tremblay, R., and Rudy, B. (2013). Neocortical somatostatin-expressing GABAergic interneurons disinhibit the thalamorecipient layer 4. Neuron *77*, 155–167.

Yang, W., Carrasquillo, Y., Hooks, B.M., Nerbonne, J.M., and Burkhalter, A. (2013). Distinct balance of excitation and inhibition in an interareal feedforward and feedback circuit of mouse visual cortex. J. Neurosci. *33*, 17373–17384.

Zhou, Y., Won, J., Karlsson, M.G., Zhou, M., Rogerson, T., Balaji, J., Neve, R., Poirazi, P., and Silva, A.J. (2009). CREB regulates excitability and the allocation of memory to subsets of neurons in the amygdala. Nat. Neurosci. *12*, 1438–1443.

Neuron, Volume *91*

Supplemental Information

Multimodal and Site-Specific Plasticity of Amygdala Parvalbumin Interneurons after Fear Learning

Elizabeth K. Lucas, Anita M. Jegarl, Hirofumi Morishita, and Roger L. Clem

Supplemental Information.

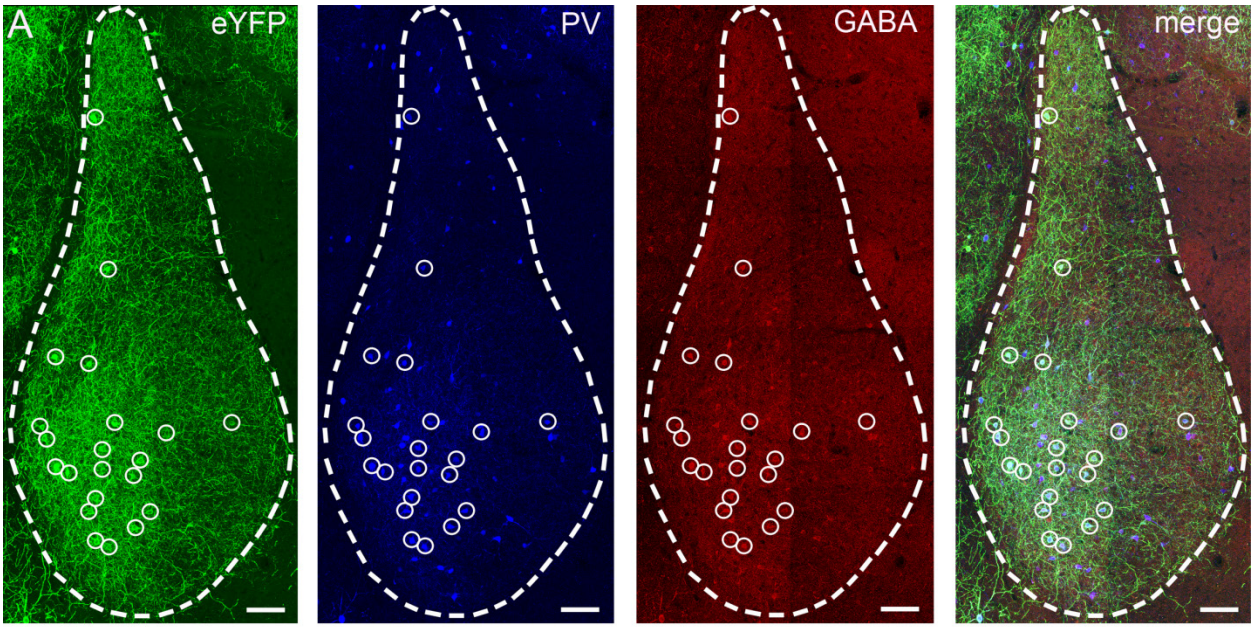

B

	Animal # 1	2	3	4	Total
PV+	118	216	176	139	649
PV+/GABA+	78	111	113	66	368
YFP+	41	69	42	32	184
YFP+/PV+	41	67	40	31	179
YFP+/GABA+	39	61	41	29	170
YFP+/PV+/GABA+	39	60	39	29	167

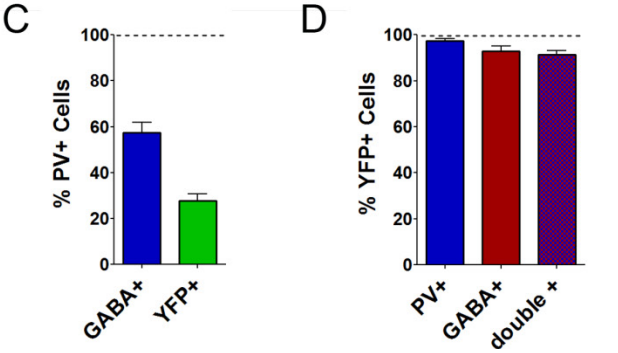

Figure S1. ***PV-IRES-Cre recombination throughout the basolateral amygdala***, related to Figure 1. PV-IRES-Cre mice were crossed to R26-stop-eYFP reporter mice to express eYFP specifically in PV-INs. **A.** Double immunofluorescence staining with antibodies against PV (blue) and GABA (red) show that Cre-dependent recombination is restricted to GABAergic PV-INs. Scales = 100 µm. **B.** Cell counts from 50 µm thick coronal sections from males at postnatal day 35. n = 4 animals, 3 sections/animal. **C.** Corresponding to a previous investigation (McDonald and Mascagni, 2001), approximately 60% of PV+ neurons coexpressed GABA in the basolateral amygdala. Approximately 30% of PV+ neurons exhibited recombination in this mouse line. **D.** The overwhelming majority of eYFP+ cells (> 90%) were GABAergic PV-INs. Data presented as mean ± SEM.

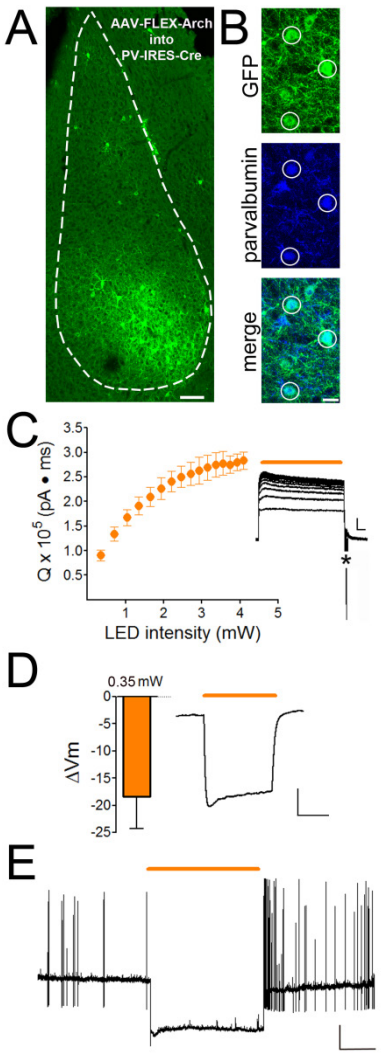

Figure S2. ***Validation of eArch3.0 in PV-INs***, related to Figure 2. **A.** AAV-Flex-Arch-GFP was injected into the basolateral amygdala of PV-IRES-Cre mice for optogenetic-assisted slice electrophysiology, scale = 100 μm. **B.** Immunofluorescence staining confirmed that GFP (green) was exclusively expressed in PV-positive neurons (blue), scale = 25 μm. **C.** Whole-cell voltage clamp recordings from GFP-positive PV-INs revealed the input-output relationship of LED intensity (λ = 590 nm) and eArch3.0 conductance. Representative traces are shown in the inset, scale = 100 pA x 50 ms. * in inset indicates rebound action currents, which have been shortened for clarity. **D.** Current clamp recordings confirmed the hyperpolarizing effect of 590 nm light. A representative trace is shown in the inset, scale = 10 mV x 250 ms. n = 4 (3). **E.** Light-induced hyperpolarization of eArch3.0-expressing PV-INs was sufficient to silence action potential generation. Scale = 15 mV x 15 ms. Data presented as mean ± SEM.

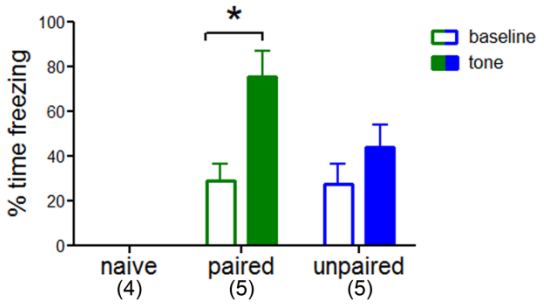

Figure S3. ***Validation of behavioral paradigm***, related to Figures 3-7**.** PV-IRES-Cre x R26-stop-eYFP mice underwent paired or unpaired auditory fear conditioning. Fear memory retrieval was assessed 24 hours later with 4 presentations of the CS, at the time point when animals were sacrificed for electrophysiological recordings. Only animals in the paired training paradigm exhibited increased freezing to the CS compared to baseline. n/group indicated on bar histogram. Two-way ANOVA; main effect of group, $F_{(2,22)} = 47.75$, $p < 0.0001$; main effect of CS, $F_{(1,22)} = 11.75$, $p < 0.007$; interaction, $F_{(2,22)} = 9.84$, $p < 0.04$. Holm-Bonferroni post-test, *$p < 0.01$. Data presented as mean ± SEM.

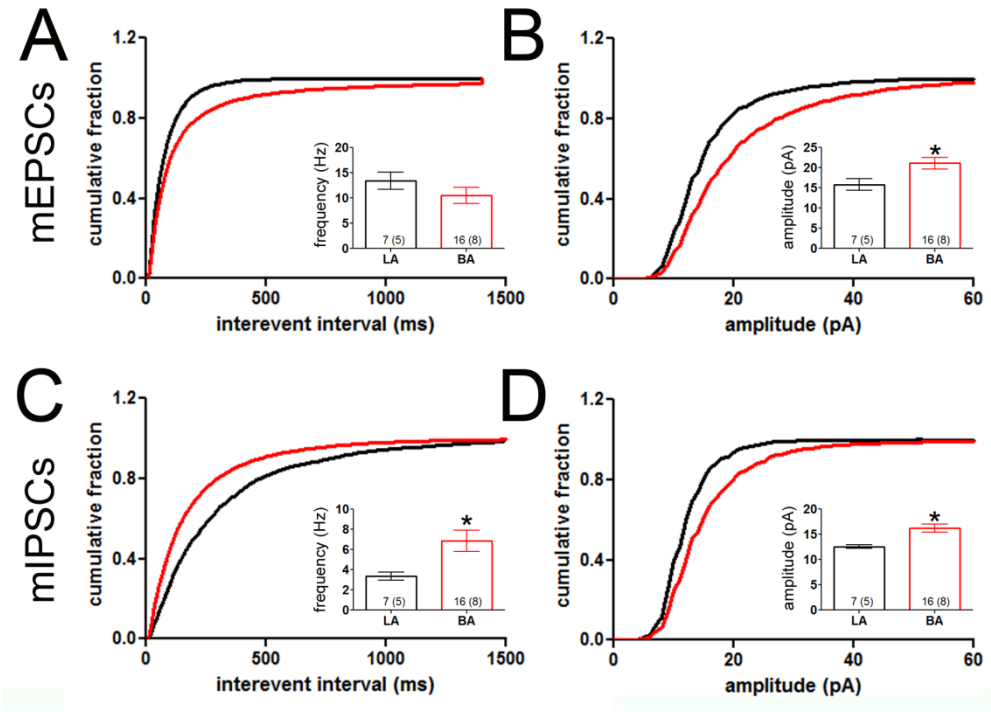

Figure S4. ***Differences in mEPSC and mIPSC frequency and amplitude in LA versus BA PV-INs***, related to Figure 3. mEPSCs and mIPSCs were isolated in PV-INs by clamping membrane potential at -60 mV and 0 mV, respectively, in the presence of a low chloride cesium internal solution. No difference in frequency (**A,** $t_{(15)}$ = 1.23, p = 0.24) but increased amplitude (**B,** $t_{(15)}$ = 2.58, p = 0.02) of mEPSCs was observed in the BA compared to LA of naïve animals. Both the frequency (**C**, $t_{(18)}$ = 3.13, p = 0.006) and amplitude (**D**, $t_{(20)}$ = 4.074, p = 0.0006) of mIPSCs was increased in the BA compared to LA of naïve animals. n/group indicated on bar histogram. Independent samples t-tests. Data presented as mean ± SEM.

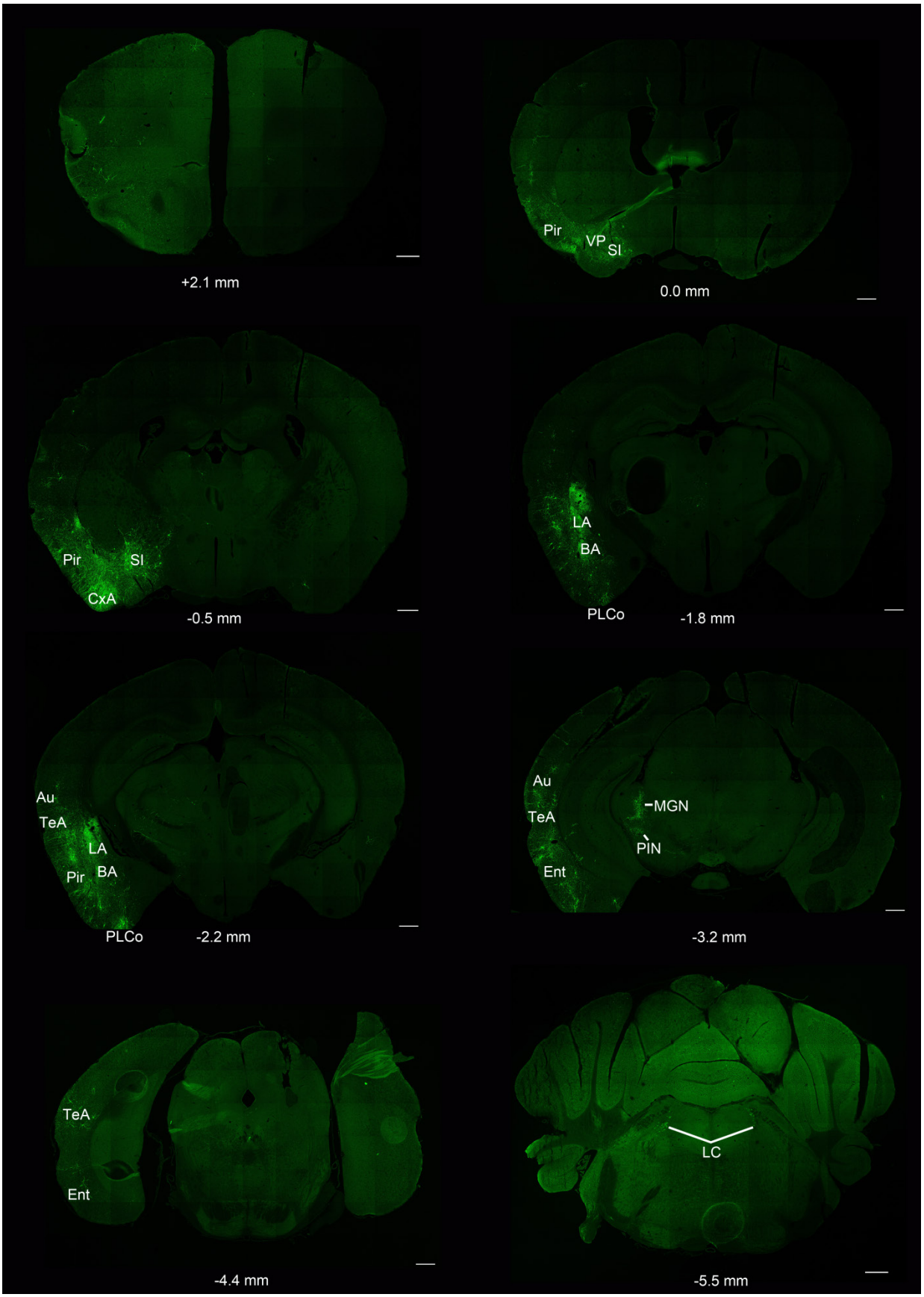
+2.1 mm
Pir
VP
SI
0.0 mm
Pir
SI
CxA
-0.5 mm
LA
BA
PLCo
-1.8 mm
Au
TeA
LA
Pir
BA
PLCo
-2.2 mm
Au
TeA
MGN
PIN
Ent
-3.2 mm
TeA
Ent
-4.4 mm
LC
-5.5 mm

Figure S5. ***Long-range innervation of amygdala PV-INs***, related to Figure 5. Four adult PV-IRES-Cre mice received unilateral basolateral amygdala infusions of AAVs encoding the conditional TVA receptor (AAV8-EF1a-FLEX-TVA-mCherry) and the rabies glycoprotein (AAV8-CA-FLEX-RG), followed by infusion of EnvA G-deleted Rabies-eGFP three weeks later. Mice were sacrificed by perfusion one week later, and GFP expression throughout the entire rostral-caudal axis of the brain was amplified with an anti-GFP antibody (green). Brain regions that were labeled in all 4 animals included the piriform (Pir) cortex, primary (Au) and secondary (TeA, temporal association cortex) auditory cortex, entorhinal (Ent) cortex, basal forebrain (VP, ventral pallidum; SI, substantia innominata), cortex-amygdala transition zone (CxA), posterolateral cortical amygdaloid nucleus (PLCo), sensory thalamus (MGN, medial geniculate nucleus; PIN, posterior intralaminar nucleus), and locus coeruleus (LC). Notably, the LC was the only bilaterally-projecting region. No GFP-labeled cells were observed in the medial prefrontal cortex of any animal. Scale bars = 500μm.

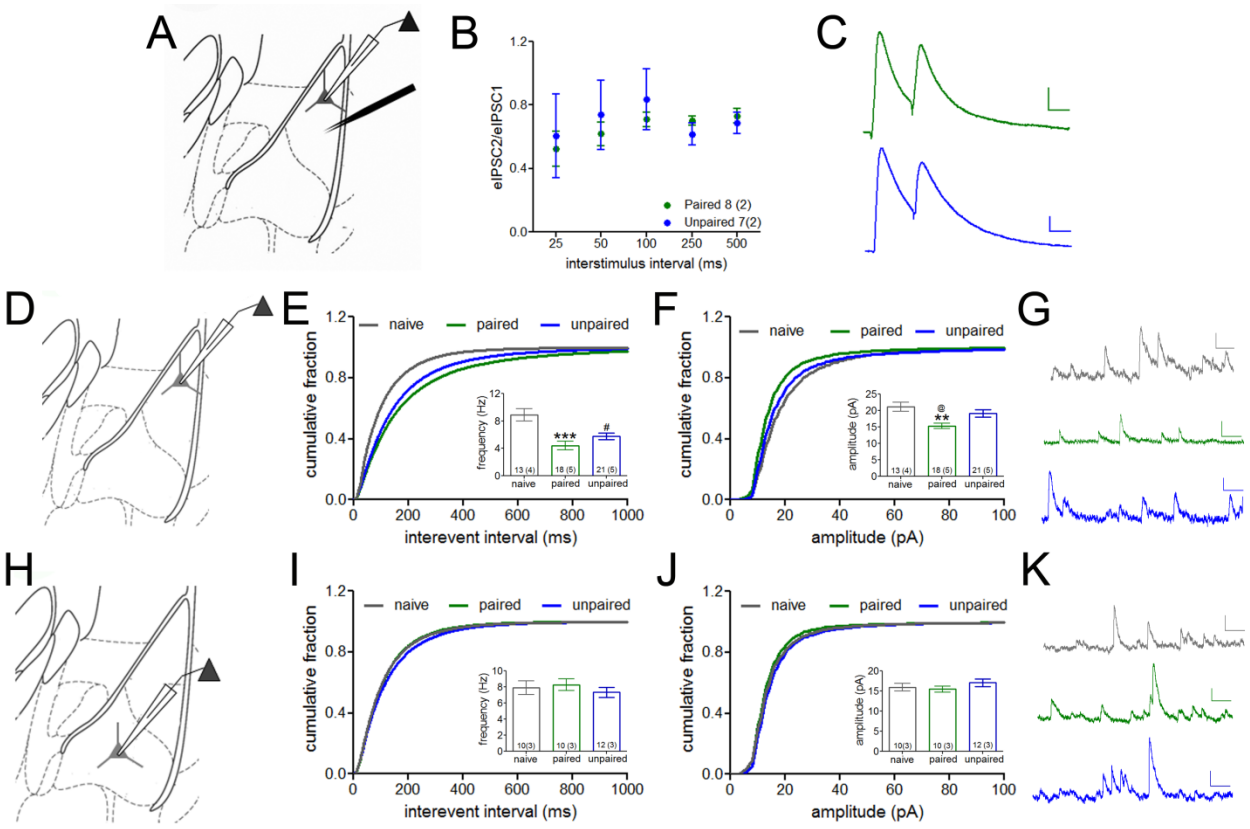

Figure S6. ***Reduced spontaneous inhibition onto principal neurons in LA but not BA after emotional learning***, related to Figure 6. **A.** In the presence of APV and CNQX, GABA release was evoked from a mixed population of local inhibitory neurons by paired-pulse stimulation during recording of IPSCs from LA principal neurons held at 0 mV. **B.** PPR (eIPSC2/eIPSC1) did not differ between paired and unpaired animals. Representative traces in **C.** Scales = 50 pA x 25 ms. **D.** Recording configuration for E-G. **E.** The frequency of sIPSCs was reduced in paired and unpaired compared to naïve animals in LA. **F.** The amplitude of sIPSCs was reduced in paired compared to naïve and unpaired animals in LA. **G** Representative traces of LA sIPSCs. **H.** Recording configuration in I-K. **I.** The frequency of sIPSCs was not changed in BA. **J.** The amplitude of sIPSCs was not changed in BA. **K.** Representative traces of BA sIPSCs. Scales G,K = 20 pA x 100 ms. n/group indicated on bar histograms. One-way ANOVA followed by Fisher's LSD. * $p < 0.05$ naïve versus paired. @ $p < 0.05$ paired versus unpaired. # $p < 0.05$ naïve versus unpaired. One symbol $p < 0.05$, two symbols $p < 0.005$, three symbols, $p < 0.0005$. Data presented as mean ± SEM.

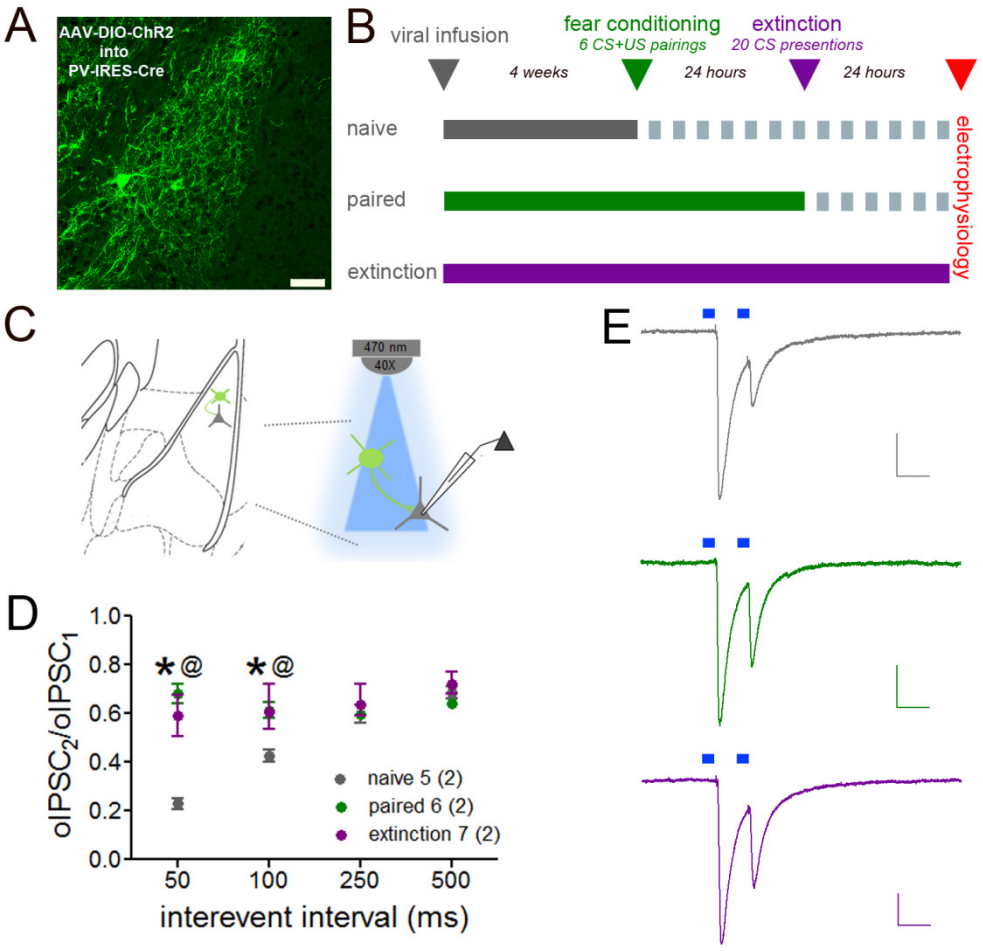

Figure S7. ***Learning-induced reduction of GABA release at PV-IN → principal neuron synapses is not reversed by extinction***, related to Figure 6**. A.** eYFP expression after viral infusion of AAV-DIO-ChR2 into the basolateral amygdala of PV-IRES-Cre mice. **B**. Experimental time line. Dashed gray line indicates the time point at which mice were sacrificed for whole-cell recordings. **C.** Experimental design. Paired pulse ratio of IPSCs evoked by blue light (λ = 470 nm) in LA principal neurons. **D.** PPR was increased in mice from the paired and extinction groups compared to the naïve group. **E.** Representative traces at the 50 ms interstimulus interval. Scales = 25 pA x 50 ms. n/group indicated on graph. Repeated-measures ANOVA; main effect of group, $F_{(2,45)} = 19.35$, $p < 0.0001$; main effect of interstimulus interval, $F_{(3, 45)} = 54.13$, $p < 0.0001$; interaction, $F_{(6,45)} = 35.57$, $p < 0.0001$. Holm-Bonferroni post-test, * $p < 0.0001$ paired versus naïve, @ $p < 0.0001$ extinction versus naïve. Data presented as mean ± SEM.

Supplemental Experimental Procedures.

Animals. All experiments were conducted on male animals 28-40 days of age. The following mouse lines were maintained on a C57Bl/6J background and obtained from Jackson Laboratories (Bar Harbor, ME, USA): C56Bl/6J (RRID:IMSR_JAX:000664), PV-IRES-Cre (RRID:IMSR_JAX:008069), R26-STOP-eYFP (RRID:IMSR_JAX:006148), and Rosa-CAG-LSL-tdTomato-WPRE (Ai9; RRID:IMSR_JAX:007909). Mice were housed 2-5 per cage with access to food and water *ad libitum* on a 12 hour light-dark cycle (lights on at 0700 hours). All experiments were approved in advance by the Institutional Care and Use Committee of the Icahn School of Medicine at Mount Sinai.

Viral targeting for electrophysiology. Viral constructs were purchased from the University of Pennsylvania Vector Core and included AAV1-EF1a-DIO-hChR2(H134R)-eYFP-WPRE (Addgene #20298), AAV1-CBA-Flex-Arch-GFP (Addgene #22222), and AAV1-CamKIIa-hChR2(H134R)-eYFP-WPRE (Addgene #26969P). Stereotaxic surgeries were conducted at 21-24 days of age. Animals were deeply anesthetized with a mixture of ketamine/xylazine (initial dose 100 mg/kg and 5 mg/kg, respectively) and mounted in a stereotaxic frame (Stoelting, Wood Dale, IL, USA). Viral constructs (0.3-1 µL) were bilaterally injected into the basolateral amygdala (AP -1.4, ML ±3.3, DV -5.0), temporal association cortex (AP -4.0, ML ±4.0, DV -3.5), and medial geniculate nucleus (AP -3.2, ML ±1.8, DV -3.5) with a motorized injector (Stoelting) at a rate of 0.1 µL per minute. After remaining in place for 15 additional minutes, the syringe was slowly retracted. Atropine (1 mg/kg) was administered during anesthesia, and post-surgery analgesia was provided with benamine (2.5 mg/kg). Mice recovered in their home cages for at least one week before experimental manipulation.

Viral targeting for monosynaptic circuit tracing. Viral constructs were purchased from the University of North Carolina Vector Core (AAV8-EF1a-FLEX-TVA-mCherry, Addgene #38044; AAV8-CA-FLEX-RG, Addgene #38043; Watabe-Uchida et al., 2012) and the Salk Institute Gene Transfer, Targeting, and Therapeutics Core (EnvA G-deleted Rabies-eGFP, Addgene #32635; Wickersham et al., 2010). Stereotaxic surgeries were conducted at 5 months of age as described above. Unilateral basolateral amygdala injections of AAV8-EF1a-FLEX-TVA-mCherry and AAV8-CA-FLEX-RG (1:1 ratio) were

conducted three weeks prior to EnvA G-deleted Rabies-eGFP, and animals were sacrificed by transcardial perfusion one week later.

Immunofluorescence staining. Mice were deeply anesthetized with a mixture of ketamine/xylazine prior to transcardial perfusion with phosphate buffered saline (PBS) and 4% paraformaldehyde (PFA). Brains were postfixed overnight in 4% PFA and either vibratome sectioned on the coronal plane at 50 µM or prepared for cryosectioning at 25 µM as previously described (Lucas et al., 2014). Immunofluorescence staining was conducted on floating or slide-mounted sections. Primary antibodies included mouse anti-parvalbumin (1:1000; Millipore, Billerica, MA, USA; RRID:AB_2174013), guinea pig anti-GABA (1:250; Millipore; RRID:AB_91011), rabbit anti-GFP (1:500, ThermoFisher Scientific, Waltham, MA, USA; RRID:AB_10073917), chicken anti-GFP (1:1,000, Millipore; RRID:AB_90890), and rabbit anti-RFP (1:1,000, ThermoFisher Scientific; RRID:AB_2315269). Fluorescence-conjugated secondary antibodies raised in goat were purchased from Jackson Immunoresearch (West Grove, PA, USA; RRIDs:AB_2338902, AB_2337972, AB_2337398, AB_2337926). After washes in PBS, slices were blocked with 10% goat serum for 1 hr at room temperature prior to overnight incubation with primary antibodies with 5% goat serum in 0.1% Triton-X PBS at 4°C. Following washes in PBS, slices were incubated with secondary antibodies with 5% goat serum in 0.1% Triton-X PBS at room temperature for 2 hr. Slices were washed in PBS, mounted onto slides (floating sections), and coverslipped with Prolong Antifade Gold with DAPI (Life Technologies, Grand Island, NY, USA). Images were captured on a Zeiss confocal microscope attached to a computer equipped with Zenn software (Carl Zeiss Microscopy, Jena, Germany). For cell counts, images were manually quantified with the ImageJ Cell Counter plugin.

Fear conditioning. Cued auditory fear conditioning was conducted in sound attenuating chambers with automated stimulus delivery software (MedAssociates, St. Albans, VT, USA). Training entailed 6 pairings of an auditory tone (CS; 2 kHz, 80 dB, 20 s) with a co-terminating scrambled footshock (US; 1 mA, 2 s). An acclimation period of 200 s in the training arena preceded the onset of cues, and CS-US pairings were separated by an 80 s inter-trial interval. Control groups included experience naïve cage mates and unpaired animals that received explicitly unpaired training (6 CS presentations followed

by 6 US presentations in discrete sessions separated by a 15 min interval in a home cage). Mice were sacrificed 24 hours after training for slice electrophysiology.

Slice electrophysiology. Mice were anesthetized with isoflurane prior to decapitation and brain removal. Acute coronal slices of the basolateral amygdala were sectioned at 350 µm on a VT1200S vibratome (Leica Microsystems, Buffalo Grove, IL, USA) in sucrose dissection solution (in mM: 210.3 sucrose, 26.2$NaHCO_3$, 11 glucose, 4 $MgCl_2$, 2.5 KCl, 1 NaH_2PO_4, 0.5 ascorbate, and 0.5 $CaCl_2$) chilled to -4°C. Slices were recovered in standard ACSF (in mM: 119 NaCl, 26.2 $NaHCO_3$, 11 glucose, 2.5 KCl, 2 $CaCl_2$, 2 MgCl2, and 1 NaH_2PO_4) for 40 min at 34°C, then maintained at room temperature for the remainder of the experiment. All solutions were continuously bubbled with 95% O_2:5% CO_2. Whole-cell recordings were obtained with borosilicate glass electrodes (resistance: 3-5 MΩ for principal neurons, 5-8 MΩ for INs) filled with voltage clamp (in mM: 120 Cs-methanesulfonate, 10 HEPES, 10 Na-phosphocreatine, 8 NaCl, 5 TEA-Cl, 4 Mg-ATP, 1 QX-314, 0.5 EGTA, and 0.4 Na-GTP), low-chloride voltage clamp (voltage clamp without TEA-Cl), and current clamp (in mM: 127.5 K-methanesulfonate, 10 HEPES, 5 KCl, 5 Na-phosphocreatine, 2 $MgCl_2$, 2 Mg-ATP, 0.6 EGTA, and 0.3 Na-GTP) internal solutions (pH 7.25; 285-300 mOsm).

Cells were visualized on an upright DIC microscope equipped with objective-coupled LEDs (460 nm and broad spectrum (white); Prizmatix, Givat-Shmuel, Israel) for the identification of fluorescence-labeled cells as well as optogenetic cellular manipulations. Principal excitatory neurons were selected based on pyramidal morphology under DIC microscopy; recordings were terminated if physiology was inconsistent with principal cells, namely capacitance less than 120 pF and fast excitatory postsynaptic current kinetics. Electrically-evoked postsynaptic currents were obtained by stimulation of the external (cortical pathway) or internal (subcortical pathway) capsule with a matrix or concentric bipolar electrode. Monosynaptic excitatory and disynaptic inhibitory postsynaptic currents in PNs and PV-INs were isolated by holding cells at -70 mV and 0 mV, respectively; compound postsynaptic currents were obtained by holding cells at -50 mV. Paired pulse ratios (PPRs) and spontaneous postsynaptic currents were obtained in picrotoxin (100 µM) for isolation of excitatory currents and in CPP (10 µM; 3-((*R*)-2-Carboxypiperazin-4-yl)-propyl-1-phosphonic acid)

and CNQX (10 μM; 6-cyano-7-nitroquinoxaline-2,3-dione) for isolation of inhibitory currents. Miniature postsynaptic currents were further isolated with tetrodotoxin (0.5 μM). Light-evoked stimulation of excitatory ChR2+ terminals evoked large polysynaptic excitatory currents in PV-INs, likely the result of feedback excitatory connections. For these experiments, saturating CPP (10 μM) and subsaturating CNQX (1 μM) was utilized to limit network excitability and thereby prevent the contamination of monosynaptic recordings with multisynaptic currents. These experiments were conducted with a low chloride cesium internal solution, which allowed for isolation of glutamatergic responses by holding the cell at -60 mV. Intrinsic excitability of PV-INs was determined by eliciting action potentials with increasing current injections (50-500 pA by 50 pA) from a resting potential of -70 mV; rheobase current was defined as the amount of current required for the generation of one action potential. The location of all cells within the basolateral amygdala was visually confirmed after recording. Data were low-pass filtered at 3 kHz (evoked) and 10 kHz (spontaneous, miniature) and acquired at 10 kHz using Multiclamp 700B and pClamp 10 (Molecular Devices, Sunnyvale, CA, USA). Evoked data were analyzed in Clampfit 10 (Molecular Devices); spontaneous and miniature currents were analyzed with MiniAnalysis (Synaptosoft, Fort Lee, NJ, USA). All data analyses were conducted blind to the experimental group.

Morphological Analysis. Live brain sections were prepared as for slice electrophysiology (see above). PV-INs were identified by tdTomato reporter expression, patched, and filled with 0.5% biocytin in voltage clamp internal solution. The location of cells within the basolateral amygdala was visually confirmed after filling. Brain slices were fixed in 4% PFA for 24 – 72 hours and stained with Alexa Flour 488-conjugated streptavidin (Johnson Immunoresearch; RRID:AB_2337249). Cells were traced on Axiophot 2 (Zeiss Microscopy, Jena, Germany) with a 40x oil immersion objective, using the Neurolucida (MBF Bioscience, Williston, VT, SA) continuous contour tracing function. The soma was traced first, using the cell body function at its brightest and most focal point. A reference point was also made at this z-level and dictated as 0.00 Z. Dendrites were traced next, using the fine focus to trace through the z-axis. Bifurcation nodes were inserted to indicate branch points in the dendritic trees. Endings were indicated as normal or incomplete; incomplete endings are indicative of truncated dendrites. Analysis was

conducted using the branched structure analysis function of Neurolucida Explorer to obtain cell perimeter data and a neuron summary, including number of dendrites, nodes, and endings.

Statistics. All statistical analyses were conducted with SPSS 20 (IBM, Armonk, NY, USA) or GraphPad Prism 5 (La Jolla, CA, USA). Two-tail paired t-tests (one group), two-tail independent samples t-tests (two groups), one-way ANOVA (≥ 3 groups), two-way ANOVA (≥ 2 groups with ≥ 2 variables), or two-way repeated-measured ANOVA (≥ 2 groups with repeating variable) were implemented to determine statistical significance. Equivalent non-parametric tests were conducted on data sets that violated assumptions of normality. All posthoc tests were chosen to maintain family wise error rate at 0.05. Data are presented as mean ± standard error of the mean (SEM) with *n* as the number of cells followed by the number of animals in parentheses.

References.

Lucas, E.K., Jegarl, A., and Clem, R.L. (2014). Mice lacking TrkB in parvalbumin-positive cells exhibit sexually dimorphic behavioral phenotypes. Behav. Brain Res. *274*, 219-225.

McDonald, A.J., and Mascagni, F. (2001). Colocalization of calcium-binding proteins and GABA in neurons of the rat basolateral amygdala. Neuroscience 105, 681–693.

Watabe-Uchida, M., Zhu, L., Ogawa, S.K., Vamanrao, A., and Uchida, N. (2012). Whole-brain mapping of direct inputs to midbrain dopamine neurons. Neuron *74*, 858-873.

Wickersham, I.R., Lyon, D.C., Barnard, R.J., Mori, T., Finke, S., Conzelmann, K.K., Young, J.A., and Callaway, E.M. (2007). Monosynaptic restriction of transsynaptic tracing from single, genetically targeted neurons. Neuron *53*, 639-647.